Conductance distribution in strongly disordered mesoscopic systems in three dimensions

K. A. Muttalib[1], P. Markoš[2] and P. Wölfle[3]
[1] *Department of Physics, University of Florida, P.O. Box 118440, Gainesville, FL 32611-8440*
[2] *Institute of Physics, Slovak Academy of Sciences - 845 11 Bratislava, Slovakia*
[3] *Institut für Theorie der Kondensierten Materie, Universität Karlsruhe, Germany*

Recent numerical simulations have shown that the distribution of conductances $P(g)$ in three dimensional strongly localized systems differs significantly from the expected log normal distribution. To understand the origin of this difference analytically, we use a generalized Dorokhov-Mello-Pereyra-Kumar (DMPK) equation for the joint probability distribution of the transmission eigenvalues which includes a phenomenological (disorder and dimensionality dependent) matrix K containing certain correlations of the transfer matrices. We first of all examine the assumptions made in the derivation of the generalized DMPK equation and find that to a good approximation they remain valid in three dimensions (3D). We then evaluate the matrix K numerically for various strengths of disorder and various system sizes. In the strong disorder limit we find that K can be described by a simple model which, for a cubic system, depends on a single parameter. We use this phenomenological model to analytically evaluate the full distribution $P(g)$ for Anderson insulators in 3D. The analytic results allow us to develop an intuitive understanding of the entire distribution, which differs qualitatively from the log-normal distribution of a Q1D wire. We also show that our method could be applicable in the critical regime of the Anderson transition.

PACS numbers: 73.23.-b, 71.30., 72.10. -d

I. INTRODUCTION

The full distribution of conductances $P(g)$ for non-interacting electrons at zero temperature has recently been studied in detail in quasi one dimension (Q1D) both analytically[1] and numerically[2,3]. Large mesoscopic fluctuations lead to several remarkable features in the distribution, including a highly asymmetric 'one-sided' log-normal distribution at intermediate disorder between the metallic and insulating limits[4,5], and a singularity in the distribution near the dimensionless conductance $g \sim 1$ in the insulating regime[6]. While some numerical studies exist for 3D finite size systems[7,8,9,10,11], there is no analytic method currently available to study the full distribution $P(g)$ in 3D, especially at strong disorder. Theoretical work based on $2+\epsilon$ dimensions ($\epsilon \ll 1$), where a weak disorder approximation can be applied, has been used to propose that the critical distribution at the Anderson transition point has a Gaussian center with power law tails[12,13], but this can not be compared with numerical results in 3D[7,8] that show a highly non-trivial asymmetric distribution similar to the one-sided log-normal form of Q1D. It has not been possible so far to study analytically even the simpler case of $P(g)$ in the deeply insulating regime in 3D, where numerical results point to non-trivial deviations from the expected log-normal form[11].

The $P(g)$ in Q1D systems were studied analytically within the transfer matrix approach[2]. In this paper we use a recently proposed generalization of the Q1D approach[14] to obtain analytically for the first time the full $P(g)$ for strongly disordered 3D systems. A brief account of the work has been published earlier[15]. In Sections II and III we review briefly the DMPK equation and its generalization, respectively. In Sect. IV we analyze in detail the numerical data for 3D disordered systems in all three transport regimes: metallic, insulating and critical. Numerical data allow us to determine the free parameters of a matrix K which appears in the generalized DMPK equation. In Sect V we use them to formulate a simple model for K, and solve the generalized DMPK equation analytically. In Sect. VI, an analytical formula for the conductance distribution $P(g)$ is derived in detail. In our model, the form of $P(g)$ is determined by two parameters, Γ, which measures the strength of the disorder, and γ_{12}, which determines the strength of the interaction term in the generalized DMPK equation. $\gamma_{12} \equiv 1$ in the Q1D systems. The fact that $\gamma_{12} < 1$ in 3D makes the statistics of the conductance in 3D different from that in Q1D. Although we introduced two new disorder dependent parameters, they turn out to be related to each other and we show that the present model is not in contradiction with the single parameter scaling theory[16]. In Sect. VII we compare the analytical formula for the conductance distribution with the numerical data and analyze how the distribution $P(\ln g)$ depends on the parameter γ_{12}. In the limit $\gamma_{12} \to 1$, we recover the Q1D results. Sect. VIII discusses the possible extension of our solution to the critical point. We show that our results describe the critical regime qualitatively correctly, including the non - analyticity of the critical conductance distribution. Finally, summary and conclusions are given in Sect. IX.

II. THE TRANSFER MATRIX APPROACH

The distribution of conductances for non-interacting electrons at zero temperature can be studied within the transfer matrix approach. In this approach, a conductor of length L_z and cross-section $L \times L$ is placed between two perfect leads; the scattering states at the Fermi energy then define $N \propto L^2$ channels. The $2N \times 2N$ transfer matrix M relates the flux amplitudes on the right of the system to those on the left[17]. Flux conservation and time reversal symmetry (we consider the case of unbroken time reversal symmetry only) restricts the number of independent parameters of M to $N(2N+1)$ and M can be written in general as[17,18]

$$M = \begin{pmatrix} u & 0 \\ 0 & u^* \end{pmatrix} \begin{pmatrix} \sqrt{1+\lambda} & \sqrt{\lambda} \\ \sqrt{\lambda} & \sqrt{1+\lambda} \end{pmatrix} \begin{pmatrix} v & 0 \\ 0 & v^* \end{pmatrix}, \quad (1)$$

where u, v are $N \times N$ unitary matrices, and λ is a diagonal matrix, with positive elements $\lambda_i, i = 1, 2, ...N$. Microscopic distribution of impurities will lead to a distribution $p_{L_z}(M)d\mu(M)$ of the transfer matrices where $d\mu(M)$ is an invariant measure which we rewrite as

$$p_{L_z}(M)d\mu(M) = p_{L_z}(\lambda, u, v)d\mu(\lambda)d\mu(u)d\mu(v). \quad (2)$$

If we know the marginal distribution

$$\bar{p}_{L_z}(\{\lambda_a\}) = \int p_{L_z}(\lambda, u, v)d\mu(u)d\mu(v), \quad (3)$$

then the distribution of conductances $P(g)$ can be written as

$$P(g) = \int \cdots \int \prod_{a=1}^{N} d\lambda_a \bar{p}_{L_z}(\{\lambda_a\}) \delta\left(g - \sum_{a=1}^{N} \frac{1}{1+\lambda_a}\right), \quad (4)$$

where

$$g = \sum_{a=1}^{N} \frac{1}{1+\lambda_a} \quad (5)$$

is the Landauer conductance[19]. A systematic approach to evaluate the N-dimensional integral, based on a mapping to a one-dimensional statistical mechanical problem, has been developed[1], so the full distribution $P(g)$ can be obtained if the marginal distribution $\bar{p}_{L_z}(\{\lambda_a\})$ is known. Note that the distribution of other transport variables which can be written as $\sum_a f(\{\lambda_a\})$, e.g. shot noise power[20] $P = \sum_{a=1}^{N} \frac{\lambda_a}{(1+\lambda_a)^2}$ or conductance of N-S (Normal metal-Superconductor) microbridge[21] $G = \sum_{a=1}^{N} \frac{1}{(1+2\lambda_a)^2}$, can also be obtained in the same way. The above approach is valid in principle for all strengths of disorder, in all dimensions.

If we assume that the distribution $p_{L_z}(\lambda, u, v)$ is *independent* of u, v, then the evolution of the distribution with length L_z can be obtained from a Fokker-Planck equation first derived by Dorokhov and by Mello, Pereyra and Kumar[18] which has become known as the DMPK equation:

$$\frac{\partial p_{L_z}(\lambda)}{\partial(L_z/\ell)} = \frac{2}{N+1}\frac{1}{J}\sum_{a}^{N} \frac{\partial}{\partial\lambda_a}\left[\lambda_a(1+\lambda_a)J\frac{\partial p}{\partial\lambda_a}\right],$$
$$J \equiv \prod_{a<b}^{N} |\lambda_a - \lambda_b|^\beta. \quad (6)$$

Here ℓ is the mean free path and the parameter β is equal to $1, 2$ or 4 depending on orthogonal, unitary or symplectic symmetry of the transfer matrices. We will consider only the case with time-reversal symmetry, for which $\beta = 1$. Although the parameters λ_a are not eigenvalues of M, it turns out that they determine the eigenvalues of the matrix $TT^\dagger$ (T is the transmission matrix[22])

$$TT^\dagger = v^*(1+\lambda)^{-1}v \quad (7)$$

which characterizes the conductance given by Eq. (5), and the matrix v contains the eigenvectors of $TT^\dagger$. So we will loosely refer to these as the eigenvalues and the eigenvectors in the text. Note that the parameter β determines the strength of 'level repulsion' between eigenvalues.

The assumption that $p_{L_z}(\lambda, u, v)$ is independent of u, v restricts the validity of the DMPK equation to quasi one dimension (Q1D). Quasi 1D means not only that $L_z \gg L$ where L_z is the direction of the current and L is the cross-sectional dimension, but it also requires that $\xi \gg L$, where ξ is the localization length. In this limit, all channels become 'equivalent', the matrices u and v become isotropic and the distribution becomes independent of u or v. The distribution of conductances $P(g)$ for such Q1D systems has been studied recently; it has many surprising features arising from large mesoscopic fluctuations. These include a highly asymmetric 'one-sided' log-normal distribution at intermediate disorder between the metallic and insulating limits[4,5], and a singularity in the distribution near $g \sim 1$ in the insulating regime[6]. It is not clear if these features persist in higher dimensions.

III. GENERALIZED DMPK EQUATION IN HIGHER DIMENSIONS

To study 3D systems, a phenomenological generalization of the DMPK equation has recently been proposed in which the Q1D restriction is lifted in favor of an unknown matrix

$$K_{ab} \equiv \langle k_{ab} \rangle_L ; \quad k_{ab} \equiv \sum_{\alpha=1}^{N} |v_{a\alpha}|^2 |v_{b\alpha}|^2, \quad (8)$$

where the angular bracket represents an ensemble average. In terms of this matrix, the marginal distribution $\bar{p}_{L_z}(\lambda)$ satisfies an evolution equation given by[14]

$$\frac{\partial \bar{p}_{L_z}(\lambda)}{\partial(L_z/\ell)} = \frac{1}{\bar{J}}\sum_{a}^{N} \frac{\partial}{\partial\lambda_a}\left[\lambda_a(1+\lambda_a)K_{aa}\bar{J}\frac{\partial \bar{p}}{\partial\lambda_a}\right],$$

$$\bar{J} \equiv \prod_{a<b}^{N} |\lambda_a - \lambda_b|^{\gamma_{ab}}; \quad \gamma_{ab} \equiv \frac{2K_{ab}}{K_{aa}}. \tag{9}$$

In Q1D under the isotropy condition, the matrix K reduces to

$$K_{ab}^{Q1D} = \frac{1+\delta_{ab}}{N+1}; \quad \gamma_{ab}^{Q1D} = 1, \tag{10}$$

and one recovers the DMPK equation (with $\beta = 1$). In 3D, K is not known analytically, and must be obtained from independent numerical studies.

There are two major assumptions made in Ref. [14] in deriving Eq. (9):

(i) the elements k_{ab} can be replaced by their mean values K_{ab}, and

(ii) the L_z-dependence of K_{ab} is negligible.

These assumptions need to be verified before the equation can be used. Note that the matrix K depends on the choice of representation. Since the assumptions are most natural in the position representation, we will study the matrix in this representation.

IV. NUMERICAL DATA

The generalized DMPK equation apparently introduces a large number of new parameters, elements of the matrix K_{ab}. There is no theoretical prediction about how these parameters should depend on the size of the system or on disorder. We only know that in the Q1D limit they should follow Eq. (10). Therefore our first goal is to study numerically various 3D and Q1D systems systematically in detail in order to answer the following questions:

Q1: Are the assumptions (i) and (ii) discussed in Section III valid at all strengths of disorder?

Q2: How do the elements K_{ab} depend on disorder and on the system size?

Q3: How do the elements K_{ab} depend on the indices a and b?

Q4: Given the size, disorder and index dependence of K_{ab}, is it possible to construct a simple model of K at all disorder with only a small number of parameters?

We will address all of the above in this section, but let us first briefly discuss the numerical procedure used to evaluate K.

We consider the tight binding Anderson model defined by the Hamiltonian

$$\mathcal{H} = W \sum_n \varepsilon_n c_n^\dagger c_n + \sum_{[nn']} t_{nn'} c_n^\dagger c_{n'}. \tag{11}$$

In Eq. (11), $n = (xyz)$ counts sites on the simple cubic lattice of the size $L \times L \times L_z$, and ε_n are random energies, uniformly distributed in the interval $[-\frac{1}{2}, \frac{1}{2}]$. The parameter W measures the strength of disorder. The Fermi energy is chosen as $E_F = 0.01$. The hopping term $t_{nn'}$ between the nearest-neighbor sites nn' is unity for hopping along the z direction and $t_{nn'} = t$ for hopping in the x and y directions. Then the dispersion relation is

$$E = 2\cos k_z + 2t\cos k_x + 2t\cos k_y \tag{12}$$

For a given cross section of the sample: $L_x = L_y = L$, k_x and k_y possess values $\pi/(L+1) \times 1, 2, \ldots L$ (we consider hard wall boundary conditions). At fixed energy E, given values of k_x and k_y determine the value of k_z, which is either real (if $|\cos k_z| < 1$) or imaginary. The latter case corresponds to closed channels which do not transmit current in perfect leads. To avoid these closed channels, which are not considered in the DMPK formulation, we use $t = 0.4$. Then the model Eq. (11) exhibits a metal-insulator transition[23] at $W_c \approx 9$. To obtain transport properties, we use the transfer matrix method of [24]. The main difference from previous works[10,11] is that we also calculate eigenvectors of the matrix $TT^\dagger$. Using Eq. (1), we calculate numerically the matrix $TT^\dagger$. Owing to Eq. (7), diagonalizing $TT^\dagger$ gives us λ as well as all elements of the matrix v.

Note that the eigenvectors depend on the representation. In the original formulation of the DMPK approach, semi-infinite leads consist of mutually independent and equivalent 1D wires. Therefore, the transfer matrix in the leads is diagonal in both channel and space representations. In numerical work, we need to distinguish between these two, since the transfer matrix is diagonal only in the channel representation. We therefore calculate the matrix $TT^\dagger$ in the channel representation, find eigenvalues and eigenvectors, and transform the latter back to the space representation to obtain the matrix v. Elements of v are then used for the calculation of the matrix K in the space representation.

We now go back and address the questions raised at the beginning of this section.

A. Q1: Validity of the assumptions (i) and (ii)

In order to check assumption (i), i.e. if the elements k_{ab} can be replaced by their average K_{ab} in 3D, we analyze the probability distribution $P(k_{ab})$. We start with the weakly disordered metallic regime. Two values of disorder were used: $W = 2$ and $W = 4$. More relevant than the actual strength of the disorder is the mean free path ℓ which can be estimated from the mean conductance[25]

$$\langle g \rangle = \frac{N}{L_z}\ell \tag{13}$$

with $N = L^2$. From the L_z dependence of $\langle g \rangle$ in Q1D systems we estimate $\ell(W = 2) \approx 9.2$ and $\ell(W = 4) \approx 1.8$, in units of the lattice spacing.

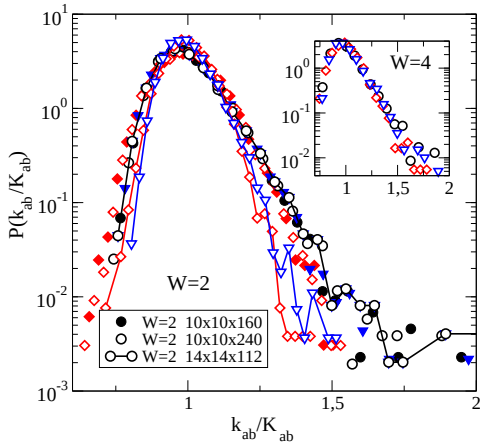

FIG. 1: Probability distribution of *normalized* k_{ab} for Q1D systems. ($\circ$: $a = b = 1$, $\diamondsuit$: $a = 1$, $b = 2$, $\bigtriangledown$: $a = b = 2$). Full symbols: $W = 2$, $L = 10$, $L_z = 16L$; open symbols: $W = 2$, $L = 10$, $L_z = 24L$. Lines with symbols: $W = 2$, $L = 14$, $L_z = 8L$. Data confirm that the distribution becomes narrower when L increases. Inset shows the same for $W = 4$ and $L = 18$, $L_z = 4L$. As expected, distributions are broader.

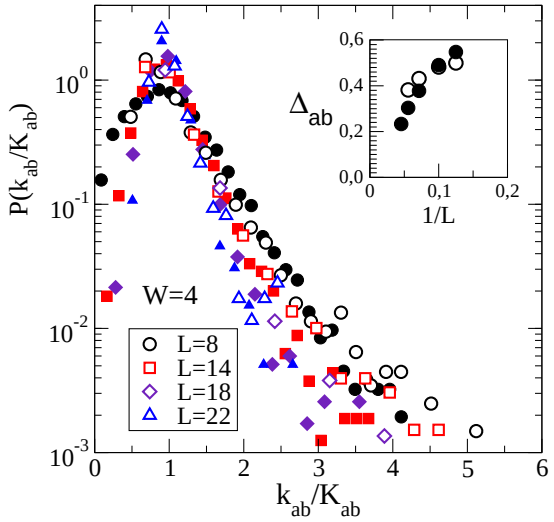

FIG. 2: The distribution of *normalized* k_{ab} for 3D systems with $W = 4$ and various system sizes. (critical disorder $W_c \approx 9$.) Open symbols: $a = b = 1$; full symbols: $a = 1$, $b = 2$. Inset shows the L-dependence of $\Delta_{ab} = \sqrt{\text{var } k_{ab}}/K_{ab}$ which decreases when L increases. Data confirm that distribution is self-averaging (it becomes narrower and $\Delta_{ab} \to 0$ when L increases) although it is broader than in the Q1D case.

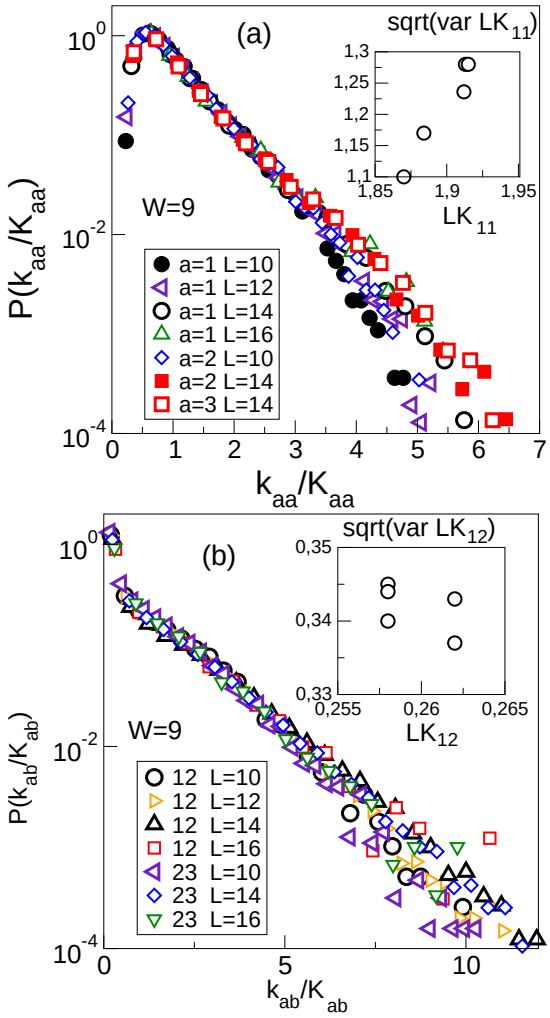

FIG. 3: Probability distribution of *normalized* matrix elements k_{ab}. (a) $P(k_{aa}/K_{aa})$ ($a = 1, 2$ and 3) at the critical point $W = W_c \approx 9$. Distribution is L-independent (apart from the exponential tail which is broader for larger L since mean value $K_{aa} \sim 1/L$). Note the logarithmic scale on the y axis. (b) Distribution of off-diagonal elements k_{12} and k_{23} possess sharp maxima close to zero, and long exponential tails. Insets show standard deviations of distributions as a function of mean values for $8 \leq L \leq 18$. These data also show the accuracy of our estimate of the critical point since we expect both the mean and the standard deviation to be L-independent at $W = W_c$. The distributions for Q1D systems $L \times L \times 8L$ are almost identical to those for cubes (data not shown).

First, we test how assumption (i) is fulfilled in the weakly disordered limit, where the DMPK equation is known to describe the universal features of transport statistics correctly. We show in Figure 1 the distribution $P(k_{ab})$ in the weakly disordered Q1D regime. As expected, the width of the distribution increases when W increases, but $P(k_{ab})$ is self-averaging (it becomes narrower when L increases). Figure 2 shows the same distribution for 3D systems. The distribution is again self-averaging, although much broader than in the Q1D case.

In the critical regime, the probability distribution $P(k_{ab})$ is no longer self-averaging but tends to be L-independent in the limit $L \to \infty$ (Fig. 3). Although the distributions possess long exponential tails, they have well defined sharp maxima, which do not depend on the system size.

In the insulating regime, the distribution $P(k_{11})$ be-

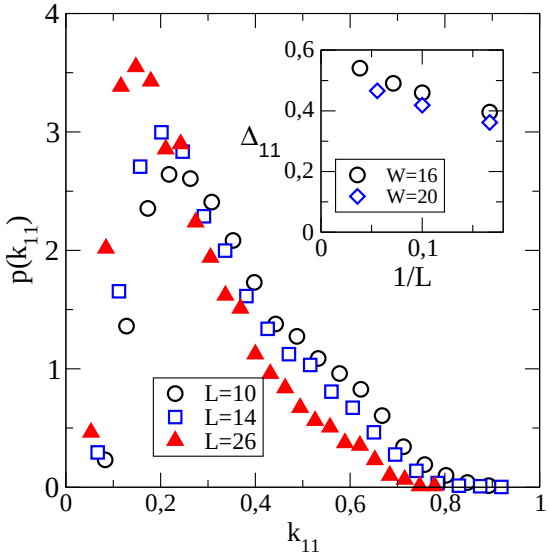

FIG. 4: Probability distribution $P(k_{11})$ in the insulating regime ($W = 16$). Although distribution becomes narrower when system size L increases, it is not self-averaging. Inset shows the size dependence of the $\Delta_{11} = \sqrt{\text{var } k_{11}}/K_{11}$ for $W = 16$ and $W = 20$. Δ_{11} converges to a non-zero constant when $L \to \infty$.

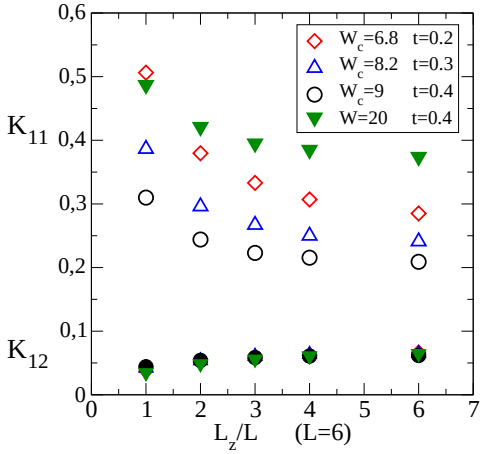

FIG. 5: At the critical point, which depends on the anisotropy parameter t, both LK_{11} and LK_{12} converge to L_z-independent values when $L_z/L \to \infty$. The limiting value LK_{11} depends on t. Shown are also data for the insulating regime $W = 20$, $t = 0.4$. All data for K_{12} almost coincide so that they are not distinguishable in the figure.

comes narrower when L increases (Fig. 4). However, on the basis of our numerical data we conclude that the distribution is not self-averaging. Although var k_{11} decreases when $L \to \infty$ (data not shown), the normalized width $\Delta_{11} = \sqrt{\text{var } k_{11}}/K_{11}$ (shown in inset of fig. 4) slightly increases when L increases. As K_{11} itself is non-zero in the limit $L \to \infty$ (fig. 9), Δ_{11} should converge to an L-independent function for large L.

The distribution of off-diagonal elements $P(k_{12})$ in the insulating regime (not shown) is qualitatively the same as that at the critical point.

We conclude that both in the critical and localized regimes the distributions converge to L independent functions with a well-defined peak, but the standard deviation is of the same order of magnitude as the mean. We note that the most-probable value of k_{11} is always very close to its mean value; we therefore expect that replacing k_{11} by its mean value K_{11} is a reasonable approximation as long as one is interested in qualitative results only. Thus, although to leading order assumption (i) remains valid for all disorder, we have to keep in mind that fluctuations of the elements k_{ab} in the strongly disordered regime might become important if the final results are sensitive to the exact values of these elements. We have checked that the final distribution of conductances do not change in any appreciable way if fluctuations of k_{11} are included by overaging the conductance distribution over $P(k_{11})$.

To check assumption (ii), namely if the L_z dependence of K_{ab} is negligible, we studied the L_z/L dependence of K_{11} and K_{12}. Figure 5 confirms that for both critical and insulating regimes the parameters K_{11} and K_{12} converge to non-zero (although t - dependent) limits when the length of the system increases. It shows that the properties of the matrix K depend only slightly on the ratio L_z/L and reach L_z-independent limiting values when $L_z/L \to \infty$ in all transport regimes. The assumption (ii) is therefore reasonably well satisfied at all disorder as long as $L_z \geq L$.

Thus we conclude from our numerical studies that to leading approximation the generalized DMPK equation (9) remains qualitatively valid at all disorder in 3D, but the effect of fluctuations of k_{ab} on the final results has to be evaluated in more detail before a quantitative comparison with numerical results can be made.

B. Q2: Disorder and size dependence of K_{ab}

We start with the weak disorder regime. To distinguish the generic W dependence of K_{11} from finite size effects, we analyzed in Fig. 6 the L dependence of the parameter

$$\kappa = (N+1)K_{11}/2. \tag{14}$$

As expected, κ decreases when L increases. However, from the analysis of Q1D systems (also shown in Fig. 6) we conclude that κ converges to 1 only for very small values of disorder. As shown in Fig. 6, $\kappa \approx 1.36$ for $W = 4$. Thus, deviations from Eq. (10) already appear in the metallic limit, probably due to the decrease of the mean free path.

In the next step we analyze how the matrix K changes when the disorder increases. Typical results are given in Fig. 7. Our data show that the L dependence of the parameters LK_{11} and γ_{12} is different for different transport regimes. While in the metallic regime LK_{11} decreases as $\sim 1/L$ and γ_{12} converges to unity when L increases, qualitatively different behavior is obtained at strong disorder.

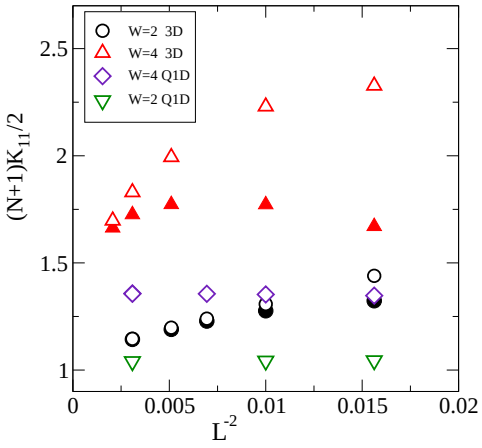

FIG. 6: $1/L^2$ dependence of $\kappa = (N+1)K_{11}/2$ (open symbols) and $(N+1)K_{12}$ (full symbols) in the metallic regime. Data confirms that κ depends on L. This agrees with data in Fig. 12. Also, $2K_{12}$ differs from K_{11} for small L. This agrees with data in Fig. 13. To estimate limiting behavior of K_{11}, we also considered Q1D systems $L \times L \times 4L$. κ is close to 1 only for very weak disorder $W = 2$. For $W = 4$ we obtained $\kappa \approx 1.36$. As this value does not depend on L for $8 \leq L \leq 18$ ($\Diamond$), we expect that 3D data for $W = 4$ will converge to the same value when $L \to \infty$.

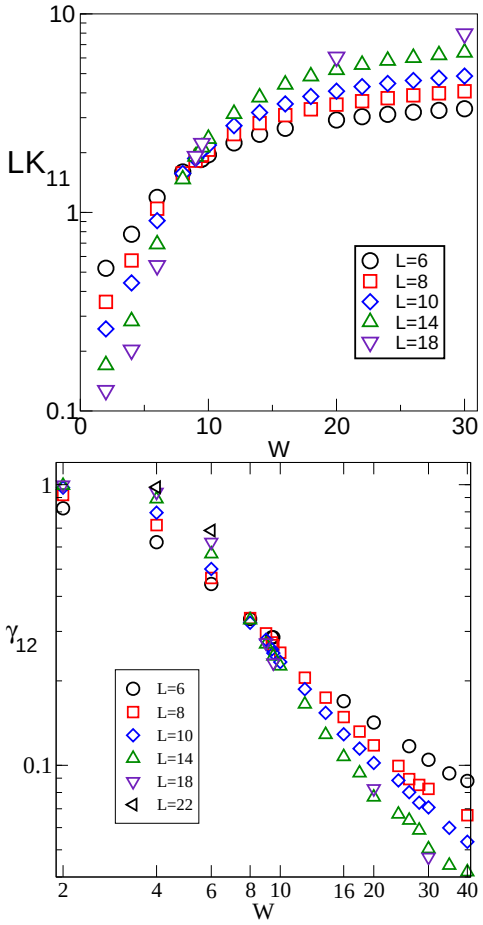

FIG. 7: Disorder dependence of K_{11} and γ_{12} for various system sizes. Note the common crossing point at $W = W_c \approx 9$. Note also that $\gamma_{12} \to 1$ for $W < W_c$ and $L \to \infty$, as expected from DMPK, but γ_{12} decreases with the system size for $W > W_c$.

In the insulating regime K_{11} converges to a non-zero L-independent constant when $L \to \infty$ (Fig. 9) and K_{12} converges to zero as $K_{12} \sim 1/L$ (Fig. 10). This means that $\gamma_{12} \sim 1/L$ in the insulating regime (Fig. 8).

Figures 7 a,b also show that there exists a critical disorder $W = W_c$ where both LK_{11} and γ_{12} are independent of L. Note that $\gamma_{12} < 1$ at $W = W_c$. We found that the critical value γ_{12c} depends on the anisotropy (Fig. 5). For the present case $t = 0.4$, $\gamma_{12c} \approx 0.28$. The qualitative L dependence in different transport regimes is summarized in Table I.

We observe that the disorder dependence of K_{11} is consistent with $K_{11} \propto 1/L^m$, where $m = 2, 1, 0$ in the metallic, critical and insulating limits, respectively, in agreement with Ref. [26]. Note that in contrast, $K_{11} \propto 1/L^2$ for all strengths of disorder in Q1D. This is a major difference between Q1D and 3D. One can understand qualitatively how the L dependence of K_{11} changes in the weak and strong disorder limits on general grounds. If all channels are equivalent, we expect the column matrix $v_{1a} \sim 1/\sqrt{N}$, which satisfies the unitary condition $\sum_{a=1}^{N} |v_{1a}|^2 = 1$. This leads to $K_{11} \sim 1/N = 1/L^2$ in the metallic limit. On the other hand, if the localization length $\xi \sim 1$, then on any cross-section at a given L_z, we expect only a few sites on the back side of the sample to be 'illuminated' by an incoming wave, so we expect $v_{1a} \sim \delta_{1a}$. This leads to $K_{11} \sim 1$, independent of L. Similarly, since all $K_{1a} \propto 1/L^2$ in the metallic regime, we expect $\gamma_{12} \sim 1$ in the metallic regime. However, in the insulating regime, we have not found a simple physical argument why $K_{12} \propto 1/L$ and hence $\gamma_{12} \propto 1/L$. We also find numerically in the insulating regime that for $1 \ll \xi \ll L$, $K_{11} \sim 1/\xi$. The structure of the eigenvector v_{1a} that gives rise to $K_{11} \sim 1/\xi$ and $K_{12} \sim 1/L$ in the region $1 \ll \xi \ll L$ is highly non-trivial, and deserves further study.

disorder	$L \times K_{11}$	γ_{12}
$W \ll W_c$	$\sim L^{-1}$	1-$\mathcal{O}(L^{-1})$
W_c	const	const
$W \gg W_c$	$\sim L$	$\sim L^{-1}$

TABLE I: Typical L-dependence of the parameters K_{11} and γ_{12} in the metallic, critical and localized regimes.

Figure 9 confirms our claim that $K_{11} > 0$ in the insulating regime. Its limiting value, $\tilde{K}_{11} = \lim_{L\to\infty} K_{11}(L)$ can be used as an order parameter for the scaling analysis of the Anderson transition. It is evident that $\tilde{K}_{11} = 0$ for $W < W_c$ and $\tilde{K}_{11} > 0$ for $W > W_c$. We show in Fig. 11 the L-dependence of LK_{11} and of the mean conductance $\langle g \rangle$ for various strengths of disorder. Similar behavior is

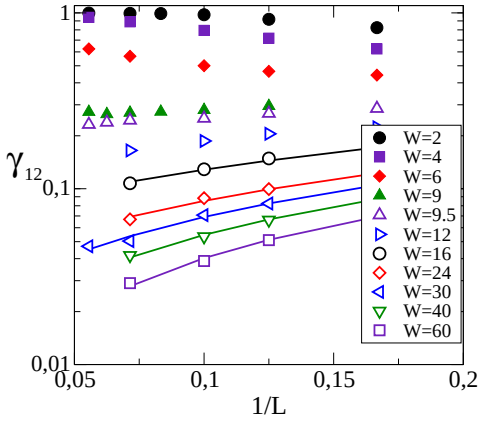

FIG. 8: γ_{12} as a function of the system size for various strengths of disorder. In the metallic regime, γ_{12} converges to 1 when $L \to \infty$. At the critical point, γ_{12} is L-independent, and in the insulating regime γ_{12} decreases when L increases. Solid lines are linear fits $\gamma_{12} = a + b/L$ with $a \sim 10^{-3}$ for $W \leq 40$.

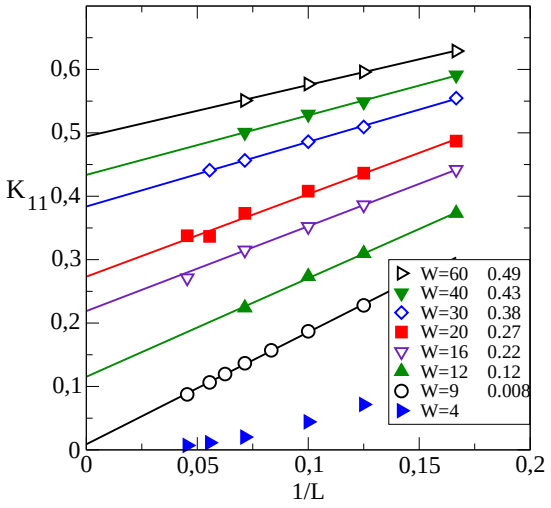

FIG. 9: System size dependence of K_{11} for various values of disorder. Solid lines are linear fits. Data in legend presents limiting values $\tilde{K}_{11} = \lim_{L\to\infty} K_{11}(L)$. Shown are also data for the metallic regime ($W = 4$) for which $K_{11} \sim 1/L^2$ (Table I). While $\tilde{K}_{11} = 0$ in metal and at the critical point ($W = 9$), it is non-zero in the insulating regime. Thus, it may be used as the order parameter of the Anderson transition.

shown in Fig. 8 for the parameter γ_{12}. One sees that all three parameters, $\langle g \rangle$, LK_{11} and γ_{12}, could be used for the estimation of the critical disorder W_c, at which none of them depends on the system size.

C. Q3: Index dependence of K_{ab}

Again we begin with weak disorder. To compare 3D and Q1D systems, we show in Fig. 12 the parameters K_{aa} as a function of the index a. It is clear that the 3D data

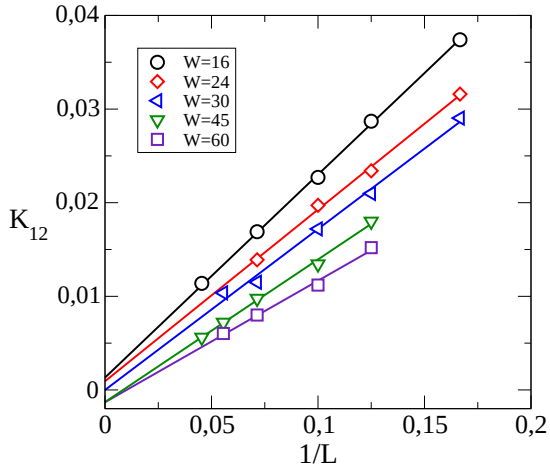

FIG. 10: System size dependence of K_{12} for various values of disorder in the insulating regime. Data confirm that $K_{12} \sim 1/L$ and that $\lim_{L\to\infty} K_{12} = 0$.

differ considerably from the DMPK value $2/(N+1)$. In Fig. 13 we show the ratio $\gamma_{1a} = 2K_{1a}/K_{11}$ for various L and compare it with Q1D numerical data. It is evident that γ_{1a} converges to 1 when the system size increases, in spite of the fact that both K_{1a} and K_{11} differ from the DMPK values of Eq. 10. The convergence is much slower in 3D than in Q1D systems. Also, γ_{1a} converges slower for larger a. We conclude that although 3D metals are qualitatively similar to Q1D metals, there are quantitative differences that need to be explored further.

In the critical regime, Figures 14 and 15 show that the a and b dependence of the matrix elements K_{ab} can be described by simple functions: $K_{aa} \sim K_{11}/a^{1/2}$, $\gamma_{1a} \sim 1/La^{1/2}$. Although we did not analyze all matrix elements in detail, we believe that the data presented here support our expectation that all matrix elements K_{ab} can be expressed in terms of K_{11}, K_{12} and some simple function of the indices a and b.

In the insulating regime we find a simple a-dependence of the *difference*

$$K_{aa} - K_{11} \approx -c\sqrt{a} \tag{15}$$

with $|c| \sim 0.04$ (Fig. 16). We also found, (Fig. 17), that for $a < N/4$, $\gamma_{1a} \sim 1/\sqrt{a}L$, very close to the value obtained at the critical point[27].

There is an interesting correspondence between the a-dependence of K_{aa} and the a-dependence of the parameters x_a defined through the parameters[2]

$$\lambda_a = \sinh^2 x_a \tag{16}$$

which is summarized in Table II.

We find that the index dependence of K_{aa} can be ignored in the metallic regime. The a-dependence is more pronounced at the critical point and in the localized regime. On the other hand, higher channels ($a \gg 1$) do not contribute to the transport either at the critical point

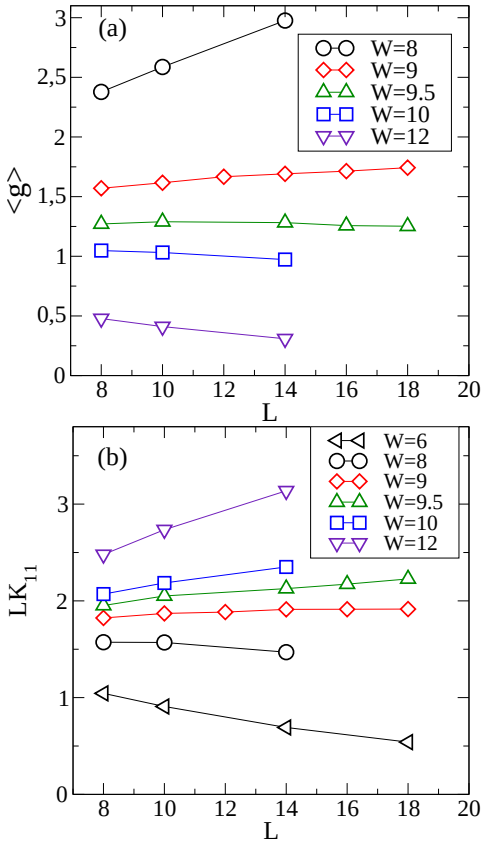

FIG. 11: Estimation of the critical point from the mean conductance $\langle g \rangle$ and from LK_{11}. Both parameters $\langle g \rangle$ and LK_{11} are L-independent at $W = W_c$. $LK_{11} \propto L$ ($\propto 1/L$) in the insulating (metallic) regime, respectively. From data we conclude that $9 < W_c < 9.5$ and use $W_c = 9$ throughout the paper.

	metal	critical point	insulator
x_a	ax_1	$\sqrt{a}x_1$	$x_1 + c\sqrt{a}$
K_{aa}	K_{11}	$K_{11}/\sqrt{a}$	$K_{11} - c/\sqrt{a}$

TABLE II: Index dependence of K_{aa} obtained in the present work compared to x_a[28] in the metallic, critical and insulating regimes.

or in the localized regime, so the actual values of K_{ab} for large a and b are not important. Therefore, we conclude that the weak index dependence of the matrix elements K_{ab} is less relevant for transport properties compared to the dependence of the matrix elements on disorder in the $L \to \infty$ limit.

It is also worth mentioning that since we are interested only in L-independent quantities at the critical point, the a-dependence of any parameter is relevant only for $a \leq L$. When a becomes comparable to L, we can not distinguish the true a-dependence from finite size effects.

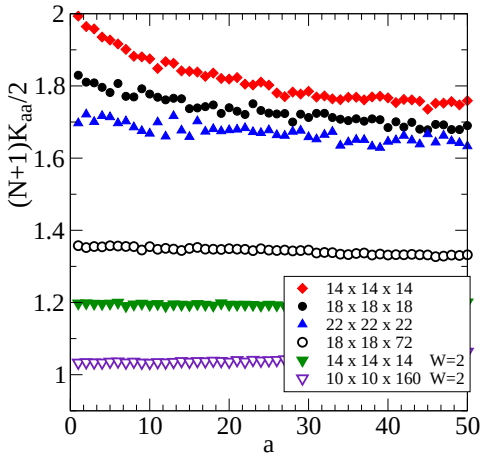

FIG. 12: a-dependence of $K_{aa} \times (N+1)/2$ for 3D and Q1D systems with $W = 2$, (mean free path $l \approx 9.2$) and for $W = 4$ ($l \approx 1.8$). K_{aa} are larger than is predicted by the DMPK theory. Good agreement with DMPK is observed only for Q1D systems with very small disorder ($W = 2$).

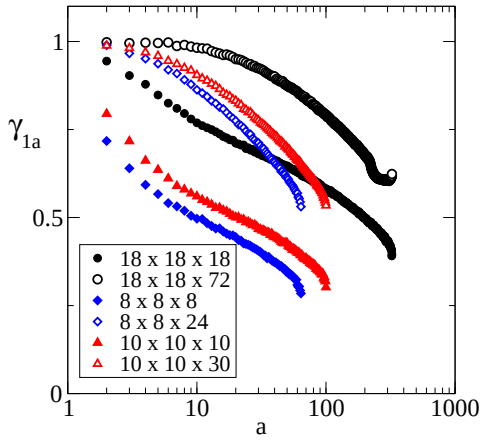

FIG. 13: a-dependence of γ_{1a} for the metallic regime ($W = 4$). Finite size effects are clearly visible so that $\gamma_{12} = 1$ only in the limit of large system size. As expected, convergence is better for Q1D systems than for cubes. Nevertheless, data confirm that γ_{1a} converge to 1 in the limit $L \to \infty$ even when K_{11} and K_{12} do not converge to values assumed by DMPK given in Eq. (10).

D. Q4: Simple model for K

Finally we ask the question if it is possible to construct a simple model of K_{ab} with only a small number of independent parameters. We just concluded in the previous section that the weak index dependence of the matrix at strong disorder is not very important. We expect that the crude approximations

$$K_{aa} \approx K_{11} \quad \text{and} \quad \gamma_{ab} \approx \gamma_{12} \tag{17}$$

capture the major qualitative features of the matrix K.

Approximation (17) introduces two new parameters, K_{11} and γ_{12}. We show that both parameters K_{11} and

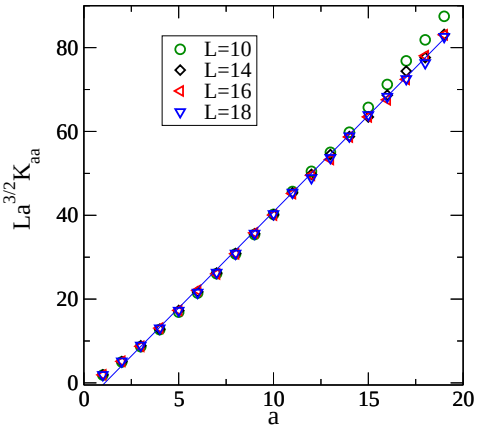

FIG. 14: Critical point: We plot $La^{3/2}K_{aa}$ to show that $LK_{aa} \propto a^{-1/2}$ are L-independent for all $a \leq 20$

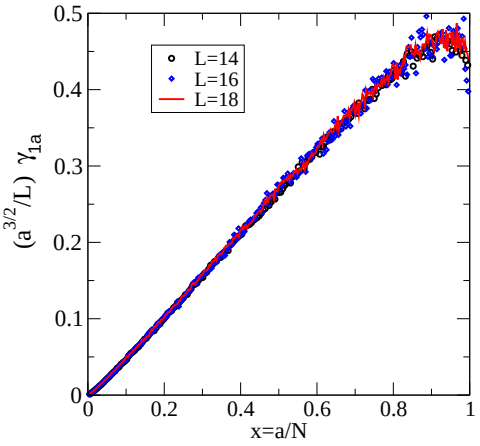

FIG. 15: Critical point. From the linear dependence $(a^{3/2}/L)\gamma_{1a} \propto a/N$ we conclude that $\gamma_{1a} \propto 1/a^{1/2}L$. ($N = L^2$)

γ_{12} are unambiguous functions of the localization length. To do so, we calculated the limiting values of K_{11} (Fig. 9) and of the parameter x_1 (Fig. 18) and plot K_{11} *versus* ξ (Fig. 19). We observe that the ξ dependence of K_{11} depends also on the anisotropy parameter t (data not shown).

In the same way, we analyzed parameter γ_{12}. As was shown in Fig. 8, we expect $\gamma_{12} \sim L^{-1}$ in the localized regime. Data in Figures 9 and 10 support this assumption. To estimate the disorder dependence of γ_{12}, we plot in Fig. 20 the quantity

$$\lim_{L\to\infty} L\gamma_{12} = 2L\ \frac{\lim_{L\to\infty} K_{12}}{\lim_{L\to\infty} K_{11}} \qquad (18)$$

which indeed increases linearly with localization length in the strongly localized regime.

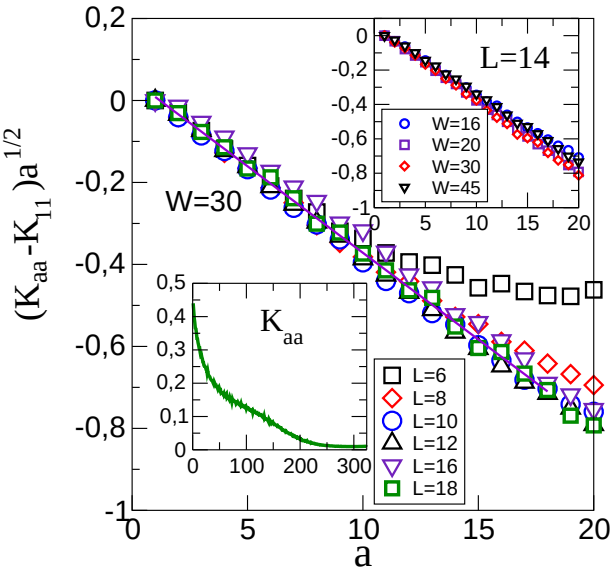

FIG. 16: Insulating regime: a-dependence of K_{aa} for 3D systems with $W = 30$. To see the a-dependence more clearly, we plot the difference $[K_{aa} - K_{11}]\sqrt{a}$ which behaves as $\sim -a$ for small a. Solid line is a linear fit, from which we have $K_{aa} = K_{11} + 0.05 - 0.04/\sqrt{a}$ for $L = 18$ and $a \leq 18$ ($K_{11} = 0.44$). Right inset presents data for $L = 14$ and various strength of the disorder. Left inset shows K_{aa} for $L = 18$.

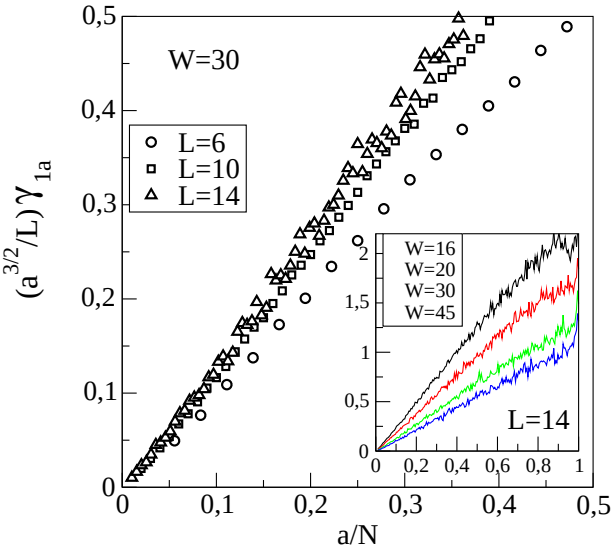

FIG. 17: Insulating regime ($W = 30$): a-dependence of γ_{1a} ($L = 6$, 10 and 14). Similar to the critical point, data shows that $a^{3/2}/L \times \gamma_{12} \sim a/N$ so that $\gamma_{1a} \sim 1/(\sqrt{a}L)$. Inset shows data for $L = 14$ and various strength of the disorder.

V. SOLUTION OF THE GENERALIZED DMPK EQUATION IN THE STRONG DISORDER LIMIT

While modeling the full γ_{ab} at the critical point needs more careful numerical studies, the insulating limit is simpler and provides a test case for the generalized

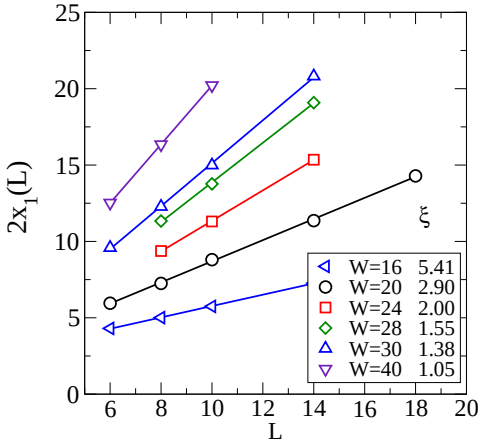

FIG. 18: Insulating regime: Estimation of the localized length $\xi(W)$ from the linear L dependence $x_1(L) = \text{const} + L/\xi$. ($\lambda_1 = \sinh^2 x_1$). Values of ξ are given in the legend. $g \approx \cosh^{-2} x_1 \approx \exp -2L/\xi$.

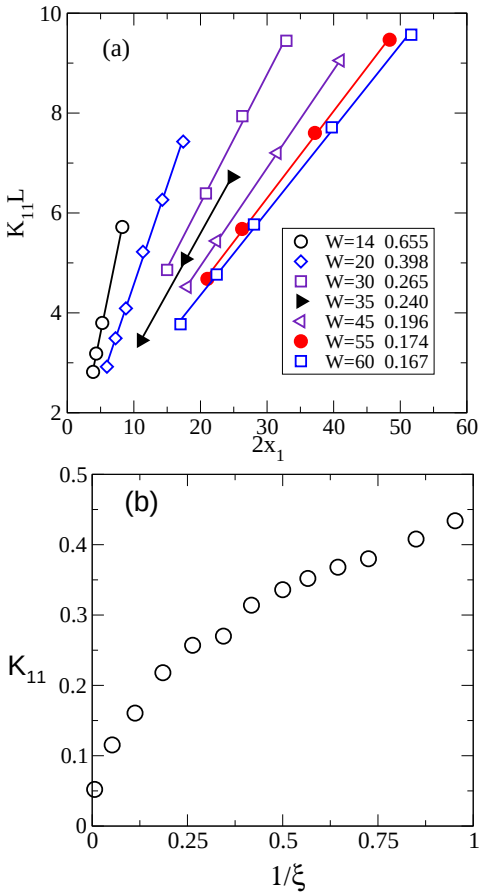

FIG. 19: Figure (a) shows how LK_{11} depends on x_1 for various disorder in the localized regime. Data confirm linear relation $LK_{11} \propto x_1$. Figure (b) shows how limiting values of K_{11}, obtained from the L-dependence of $K_{11}(L)$ (Fig. 9), depend on values of $1/\xi$ (Fig. 18). Data confirms that there is an unambiguous ξ-dependence of K_{11}.

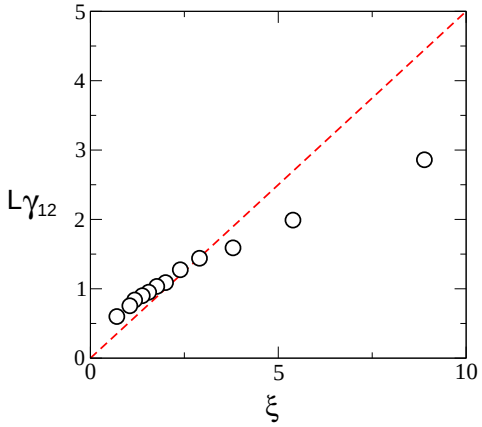

FIG. 20: $L\gamma_{12}$ defined by Eq. (18) as a function of ξ. Data confirms that there is an unambiguous ξ-dependence of γ_{12}. This is important for the formulation of the single parameter scaling theory. Dashed line is the linear dependence $\gamma_{12} = \xi/2L$, considered in [15].

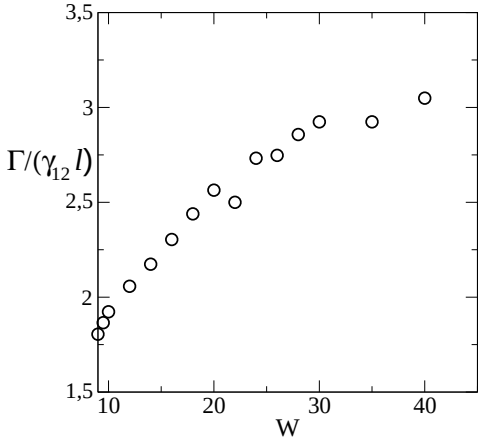

FIG. 21: Ratio $\Gamma/(\gamma_{12}\ell) = 1/2LK_{12}$, given by Eq. 21 for a cubic system, as a function of disorder for 3D systems in the insulating regime $W > W_c$.

DMPK equation (8). It predicts that the logarithmic interaction between the transmission eigenvalues λ_a vanishes as $1/L$ in the insulating limit. In the rest of the paper we will test this prediction by evaluating the full distribution of conductances in the insulating limit for a 3D conductor as described by Eq. (8), using the simple approximate model for K suggested by our numerical studies, namely

$$K_{aa} \approx K_{11} \quad \text{and} \quad \gamma_{ab} \approx \gamma_{12} \sim \text{const.}\frac{\xi}{L}. \tag{19}$$

It is useful to introduce another parameter,

$$\Gamma = \frac{\ell}{L_z K_{11}} \tag{20}$$

and the ratio

$$\frac{\Gamma}{\gamma_{12}} = \frac{\ell}{L_z K_{11}\gamma_{12}} = \frac{L}{L_z}\,\frac{\ell}{2LK_{12}}. \tag{21}$$

$\Gamma \sim 1/L_z \ll 1$ in the insulating regime, both in 3D ($L = L_z$) and Q1D ($L_z \gg L$) systems. It measures the strength of the disorder. The ratio Γ/γ_{12} reduces to Γ in the Q1D limit when $\gamma_{12} = 1$. For 3D ($L_z = L$) we see in Fig. 21 that $\Gamma/\gamma_{12} \sim L\ell/L_z$ varies smoothly between about 2ℓ and 3.5ℓ when disorder increases from W_c to infinity. Thus, the strength of disorder is characterized predominantly by the parameter Γ. For definiteness, we will use $\Gamma/\gamma_{12} = 2$ appropriate for a cubic system when needed for comparison with numerical results[29].

Note that fluctuations in k_{aa}, ignored in the model, would lead to fluctuations of Γ and γ_{12} as well, but will not change either the length or the disorder dependence of these parameters.

A brief description of the results has appeared in [15]. Here we provide many of the details.

We rewrite the generalized DMPK as[14]

$$\frac{\partial p_s(x)}{\partial(L_z/\ell)} = \frac{1}{4}\sum_a K_{aa}\frac{\partial}{\partial x_a}\left[\frac{\partial p}{\partial x_a} + p\frac{\partial \Omega}{\partial x_a}\right] \tag{22}$$

where

$$\Omega \equiv -\sum_{a<b}^{N} \ln|\sinh^2 x_b - \sinh^2 x_a|^{\gamma_{ab}} - \sum_{a=1}^{N} \ln\sinh 2x_a. \tag{23}$$

We define $P = e^{-\Omega/2}\Psi$. Then following [30], Ψ satisfies the imaginary time Schrodinger equation $-\partial\Psi/\partial(L_z/\ell) = (\mathcal{H} - U)\Psi$ with

$$\begin{aligned}\mathcal{H} = & -\frac{K_{11}}{4}\sum_a\left[\frac{\partial^2}{\partial x_a^2} + \frac{1}{\sinh^2 2x_a}\right] \\ & +\eta\sum_{a<b}\left[\frac{1}{\sinh^2(x_a - x_b)} + \frac{1}{\sinh^2(x_a + x_b)}\right],\end{aligned} \tag{24}$$

and U constant, where the strength of the interaction is given by

$$\eta = \frac{K_{11}}{4}\gamma_{12}(\gamma_{12} - 2). \tag{25}$$

The interaction term in Q1D vanishes for the unitary case, when $\gamma_{12}^{Q1D} = \beta = 2$. Note that the interaction also vanishes in the limit $\gamma_{12} \to 0$. In the 3D insulating case, $\gamma_{12} \sim \xi/2L \ll 1$, and the interaction can be considered negligible, for all symmetries. We can therefore use the $\gamma_{12} = 2$ solution of [30] for our 3D insulators. The solution in the insulating limit is then given by[30] $P = e^{-H}$, with

$$\begin{aligned}H = & -\sum_{a>b}^{N}\left[\frac{1}{2}\ln|\sinh^2 x_b - \sinh^2 x_a|^{\gamma_{12}} + \ln|x_b^2 - x_a^2|\right] \\ & -\sum_{a=1}^{N}\left[\frac{1}{2}\ln\sinh 2x_a + \ln x_a - \Gamma x_a^2\right].\end{aligned} \tag{26}$$

The replacement of $\beta = 2$ in Ref. [30] by $\gamma_{12} \to 0$ in Eq. (26) has the consequence that while all $\langle x_a\rangle \gg 1$ in the insulating regime, the difference $s = \langle x_{a+1} - x_a\rangle$ is *not* of the same order as $\langle x_a\rangle$. For example, if we keep only the first two levels, the saddle-point solutions for x_1 and x_2 give $\langle x_1\rangle \sim L_z/\xi$ and $\langle x_2 - x_1\rangle \ll \langle x_1\rangle$. We therefore do not assume that $x_2 \gg x_1$. However, we do make the simplifying approximation that $\ln|\sinh^2 x_a - \sinh^2 x_b| \approx \ln\sinh^2 x_a$ and $\ln|x_a^2 - x_b^2| \approx \ln x_a^2$ for $a > 2$ and $a > b$. Eq. (26) then becomes

$$H \approx H_1 + \sum_{a=2}^{N}\left[V(x_a) - \gamma_{12}(a-2)f(x_a)\right], \tag{27}$$

where

$$H_1 = -\ln|x_2^2 - x_1^2| + \Gamma x_1^2 - \frac{1}{2}\ln\sinh 2x_1 - \ln x_1, \tag{28}$$

$$V(x) = \Gamma x^2 - \frac{1}{2}\ln\sinh 2x - \ln x - \gamma_{12}\ln\sinh x, \tag{29}$$

$$f(x) = \ln\sinh x + k\ln x; \quad k = \frac{2}{\gamma_{12}}. \tag{30}$$

We can now use the method developed in Refs. [1,4] to obtain the full distribution $P(g)$.

VI. $P(g)$ IN 3D IN THE INSULATING LIMIT

As in [1,4], we separate out the lowest level x_1 and treat the rest as a continuum beginning at a point x_2. Then

$$H = H_1 + \int_{x_2}^{b} dx'\sigma(x')\left[V(x') - \gamma_{12}f(x')\int_{x_2}^{x'} dx''\sigma(x'')\right] \tag{31}$$

where we have used

$$(a-2) = \int_{x_2}^{x} dx'\sigma(x'). \tag{32}$$

The density satisfies the normalization condition

$$\int_{x_2}^{b}\sigma(x)dx = N - 1. \tag{33}$$

$P(g)$ can be obtained from $H(\{x_a\})$ as

$$P(g) = \int\cdots\int\prod_a dx_a e^{-H}\delta(g - \sum_a \mathrm{sech}^2 x_a) \tag{34}$$

where the δ-function represents the Landauer formula for conductance. It turns out that because of the nonlinear dependence of the Hamiltonian on the density, the complex delta function representation used in [1,4] is not suitable for the present case. We therefore use a real representation

$$\delta(x-a) = \lim_{\lambda\to 0}\frac{1}{\lambda\sqrt{\pi}}e^{-(x-a)^2/\lambda^2}. \tag{35}$$

Following [1,4], $P(g)$ may be expressed as

$$P(g) = \int D[\sigma(x)] \int_0^\infty dx \int_{x_1}^\infty dx_2 e^{-F(x_1,x_2;\sigma(x))} \quad (36)$$

where the free energy functional F is given by

$$\begin{aligned} F = \; & H_1 + \int_{x_2}^b dx' \sigma(x') \left[V(x') - \gamma_{12} f(x') \int_{x_2}^{x'} dx'' \sigma(x'') \right] \\ & + \frac{1}{\lambda^2} \left[(g - h_1) - \frac{\kappa}{2} \right]^2 \end{aligned} \quad (37)$$

where

$$\kappa \equiv 2 \int_{x_2}^b dx' \sigma(x') h(x') \quad (38)$$

and

$$h(x) \equiv \mathrm{sech}^2 x; \quad h_1 \equiv \mathrm{sech}^2 x_1. \quad (39)$$

The saddle point density is to be obtained by minimizing F with respect to $\sigma(x)$, subject to the normalization condition. We therefore define

$$\mathcal{F} \equiv F - \Lambda \left[\int_{x_2}^b \sigma(x) dx - (N-1) \right] \quad (40)$$

and minimize $\mathcal{F}$. It is useful to rewrite the free energy using the normalization condition in a way that removes the upper limit from the resulting equation. We use

$$\begin{aligned} & \frac{\delta}{\delta \sigma} \int_{x_2}^b dx' \sigma(x') f(x') \int_{x_2}^{x'} dx'' \sigma(x'') \\ = \; & \frac{\delta}{\delta \sigma} \int_{x_2}^b dx' \sigma(x') f(x') \left[(N-1) - \int_{x'}^b dx'' \sigma(x'') \right] \\ = \; & f(x) \int_{x_2}^x dx' \sigma(x') - \int_{x_2}^x dx' \sigma(x') f(x') \end{aligned} \quad (41)$$

to obtain

$$Y(x) - \Lambda = \gamma_{12} \left[f(x) \int_{x_2}^x dx' \sigma(x') - \int_{x_2}^x dx' \sigma(x') f(x') \right] \quad (42)$$

where we have defined

$$Y(x) \equiv V(x) - \frac{2}{\lambda^2} \left[(g - h_1) - \frac{\kappa}{2} \right] h(x). \quad (43)$$

Eq. (42) evaluated at $x = x_2$ fixes $\Lambda = Y(x_2)$. Taking a derivative of Eq. (42) with respect to x (represented by a prime) gives

$$Y'(x) = \gamma_{12} f'(x) \int_{x_2}^x \sigma(y) dy \quad (44)$$

Evaluated at $x = x_2$, this fixes x_2 as the beginning of the continuum

$$Y'(x_2) = 0. \quad (45)$$

Taking another derivative with respect to x, it is now possible to obtain the density

$$\sigma(x) = \frac{1}{\gamma_{12}} \left(\frac{Y'(x)}{f'(x)} \right)'. \quad (46)$$

We check that plugging $\sigma(x)$ in Eq. (46) back to Eqs. (42, 44) satisfy those equations. The density has the form

$$\sigma(x) = a_1(x) - \frac{1}{\lambda^2} a_2(x) + \frac{\kappa}{\lambda^2} b(x). \quad (47)$$

Plugging this form in the definition of κ, we obtain

$$\kappa = \frac{2 \int_{x_2}^b h(x) [a_1(x) - \frac{1}{\lambda^2} a_2(x)] dx}{1 - \frac{2}{\lambda^2} \int_{x_2}^b h(x) b(x) dx} \quad (48)$$

which, expanded in powers of λ, is given by

$$\kappa = 2(g - h_1) + \lambda^2 \mu_1 + O(\lambda^4). \quad (49)$$

where

$$\mu_1 \equiv \frac{1}{\beta} [-\alpha_1 + 2(g - h_1)] \quad (50)$$

and

$$\begin{aligned} \alpha_1 \equiv \; & \frac{2}{\gamma_{12}} \int_{x_2}^b dx \left(\frac{V'(x)}{f'(x)} \right)' h(x) \\ \beta \equiv \; & \frac{2}{\gamma_{12}} \int_{x_2}^b dx \left(\frac{h'(x)}{f'(x)} \right)' h(x). \end{aligned} \quad (51)$$

Using the expansion for κ, given by Eq. (48), we obtain in the limit $\lambda \to 0$ from Eq. (42)

$$Y(x) = V(x) + \mu_1 h(x). \quad (52)$$

The free energy can then be written as

$$F(x_1, x_2) = H_1 + \int_{x_2}^b dx \sigma(x) \left[V(x) - f(x) \frac{Y'(x)}{f'(x)} \right]. \quad (53)$$

There are two additional constraints that were not included in the variational scheme and will be enforced directly,

$$\sigma(x_2) \geq 0; \quad x_2 > x_1. \quad (54)$$

The conductance distribution now becomes

$$P(g) = \int_0^b dx_1 \int_{x_1}^b dx_2 e^{-F(x_1,x_2;g)} \delta(Y'(x_2)), \quad (55)$$

with equations (29), (30), (46) and (52) defining $V(x)$, $f(x)$, $\sigma(x)$, and $Y(x)$, respectively.

A. The free energy

Let us write $F(x_1,x_2)=H_1(x_1,x_2)+F_2(x_2)$ and define

$$W(x)=Y'(x)/f'(x). \tag{56}$$

Then $\sigma(x)=W'(x)/\gamma_{12}$ and

$$F_2=\frac{1}{\gamma_{12}}\left[\int_{x_2}^{b}dxW'(x)V(x)-\int_{x_2}^{b}dxW'(x)f(x)W(x)\right]. \tag{57}$$

On the other hand, defining

$$\Phi(x)=V(x)-f(x)W(x) \tag{58}$$

and using partial integration, we get

$$F_2=-\frac{1}{\gamma_{12}}\int_{x_2}^{b}dxW(x)\left[V'(x)-f'(x)W(x)-f(x)W'(x)\right], \tag{59}$$

where we have neglected an irrelevant term $\Phi(b)W(b)/\gamma_{12}$ independent of x_2 and we have used $W(x_2)=0$. Using $f'(x)W(x)=Y'(x)$ and $V'(x)-Y'(x)=-\mu_1 h'(x)$, we rewrite the above as

$$F_2=\frac{\mu_1}{\gamma_{12}}\int_{x_2}^{b}dxh'(x)W(x)+\frac{1}{\gamma_{12}}\int_{x_2}^{b}dxf(x)W'(x)W(x). \tag{60}$$

The two alternate expressions for F_2 can now be combined to obtain

$$\begin{aligned}\textstyle\int_{x_2}^{b}dxf(x)W'(x)W(x)=&\ \frac{1}{2}\int_{x_2}^{b}dxW'(x)V(x)\\ &-\ \frac{\mu_1}{2}\int_{x_2}^{b}dxh'(x)W(x)+C,\end{aligned} \tag{61}$$

where C is a constant. Plugging this back to Eq. (60), we obtain

$$F_2=\frac{1}{2\gamma_{12}}\int_{x_2}^{b}dxW'(x)V(x)+\frac{\mu_1}{2\gamma_{12}}\int_{x_2}^{b}dxh'(x)W(x). \tag{62}$$

We can again use partial integration to rewrite the first term as an integral over $V'(x)W(x)$, using again the fact that $W(x_2)=0$. Then the two terms can be combined to obtain

$$F_2=-\frac{1}{2\gamma_{12}}\int_{x_2}^{b}\frac{dx}{f'(x)}\left[V'^2(x)-\mu_1^2h'^2(x)\right]. \tag{63}$$

We define

$$\begin{aligned}J_1&=\int_{x_2}^{b}dx\frac{V'^2(x)}{f'(x)};\quad J_2=\int_{x_2}^{b}dx\frac{V'(x)h'(x)}{f'(x)};\\ J_3&=\int_{x_2}^{b}dx\frac{h'^2(x)}{f'(x)}.\end{aligned} \tag{64}$$

Then

$$F_2=-\frac{1}{2\gamma_{12}}[J_1-\mu_1^2J_3];\quad \mu_1=-\frac{V'(x_2)}{h'(x_2)} \tag{65}$$

B. The constraints

We already have one constraint $Y'(x_2)=0$. We also demand $\sigma(x_2)\geq 0$ which requires

$$Y''(x_2)\geq 0. \tag{66}$$

This defines x_{2min}. Also, from Eq. (50),

$$g-1/\cosh^2 x_1=\frac{1}{2}(\alpha_1+\mu_1\beta)\equiv g_0, \tag{67}$$

or

$$x_1=\cosh^{-1}\frac{1}{\sqrt{g-g_0}}. \tag{68}$$

On the other hand defining $W_1(x)=V'(x)/f'(x)$ and $W_2(x)=h'(x)/f'(x)$, it is easy to see that

$$g_0=\int_{x_2}^{b}dxh(x)\sigma(x). \tag{69}$$

Using partial integration and the fact that $Y'(x_2)=0$, we can also rewrite

$$g_0=-\frac{1}{\gamma_{12}}[J_2+\mu_1J_3]. \tag{70}$$

C. Validity of the approximations

We started with the assumption that while $\langle x_1\rangle\gg 1$ in the insulating regime, the difference $\langle x_2-x_1\rangle\ll\langle x_1\rangle$. It is therefore important to estimate the difference from the above results. We will use saddle points of the free energy

$$\begin{aligned}F(x_1,x_2)\approx&\ V(x_1)-\ln(x_2^2-x_1^2)+F_2(x_2);\\ &V(x_1)=\Gamma x_1^2-x_1-\ln x_1\end{aligned} \tag{71}$$

where F_2 is given in Eq. (63). Let us define $s=x_2-x_1$ and $\zeta=x_1-1/2\Gamma$. We assume $s\ll x_1$ and $\zeta\ll x_1$. The saddle point solutions for s and ζ are obtained from $\partial F/\partial\zeta=0$ and $\partial F/\partial s=0$. Using chain rule to write the partial derivatives in terms of $\partial F/\partial x_1$ and $\partial F/\partial x_2$ we obtain

$$V'(x_1)-\frac{2}{x_2+x_1}+F_2'(x_2)=0;\quad -\frac{1}{s}-\frac{1}{x_2+x_1}+F_2'(x_2)=0 \tag{72}$$

where prime denotes derivatives with respect to the arguments. Combining the two gives

$$-\zeta s\approx\frac{1}{2\Gamma},\quad \Gamma\ll 1. \tag{73}$$

From the definition of F_2 we have

$$F_2'(x_2)=-\frac{1}{2\gamma_{12}}\left[\frac{\partial J_1}{\partial x_2}-\mu_1^2\frac{\partial J_3}{\partial x_2}\right]+\frac{\mu_1}{\gamma_{12}}\frac{\partial\mu_1}{\partial x_2}J_3. \tag{74}$$

The integrals J_1 and J_3 depend on x_2 only via the lower limits of the integrals. Derivatives w.r.t. x_2 are simply the negatives of the integrands evaluated at the lower limit. Using definition of μ_1 this gives the first term in Eq. (74) equal to zero, leaving $F_2'(x_2) = \frac{\mu_1}{\gamma_{12}} \frac{\partial \mu_1}{\partial x_2} J_3$. Using $h(x) \approx 4e^{-2x}$ and $1/f'(x) \approx x/k$ for $x/k \ll 1$, we get

$$J_3 \approx \frac{1}{k} \left[16 x_2 e^{-4x_2} + 4e^{-4x_2}\right]. \tag{75}$$

Then

$$F_2'(x_2) \approx \Gamma^2 x_2^3 - \Gamma_3 x_2^2 + \frac{1}{4}(1+\Gamma_2) x_2 + \frac{9}{16}(1+\Gamma_1), \tag{76}$$

where $\Gamma_3 = \Gamma(1 - 3\Gamma/4)$, $\Gamma_2 = -6\Gamma + \Gamma^2/2)$ and $\Gamma_1 = -\Gamma/3$. We neglect $1/(x_2 + x_1)$ compared to the other terms in $F'(s) = 0$ (Eq. (72)) and expand $F_2'(x_2)$ in Taylor series around $x_2 = 1/2\Gamma$. The dominant term is $\frac{1}{2}(\zeta + s)^2 \Gamma$ where we have used $F_2'''(x_2 = 1/2\Gamma) = \Gamma$. Using $\zeta = -1/2\Gamma s$, we finally obtain

$$\frac{\partial F}{\partial s} \approx \frac{1}{8\Gamma s^2} - \frac{1}{2} + \frac{1}{2}\Gamma s^2 = 0. \tag{77}$$

Therefore, the saddle point solutions are given by

$$s = -\zeta = \frac{1}{\sqrt{2\Gamma}}. \tag{78}$$

Since $\langle x_1 \rangle \sim 1/2\Gamma$, we confirm our expectation that $\langle x_2 - x_1 \rangle \ll \langle x_1 \rangle$. The results are also consistent with our assumption that both s and ζ are much smaller than x_1, so the free energy calculations remain valid.

However, numerically we find that while $\langle x_1 \rangle \sim 1/2\Gamma$, $s \sim 1$ independent of disorder. Thus our result $s = \frac{1}{\sqrt{2\Gamma}} \ll \langle x_1 \rangle$ is only qualitatively correct. The fact that actual s is much smaller than what we find is related to the inaccuracy in our evaluation of the density. Indeed, we can obtain the density directly from Eq. (46). In the limit $x \gg 1$, $\gamma_{12} \ll 1$ we find

$$\begin{aligned} \sigma(x) \;&\approx \tfrac{1}{\gamma_{12}} \Big[2\Gamma - \tfrac{k(2\Gamma k+1)}{(x+k)^2} \\ &\quad + 2V'(x_2) \left(\tfrac{x}{x+k} - \tfrac{k}{2(x+k)^2} \right) e^{-2(x-x_2)} \Big] \end{aligned} \tag{79}$$

where we have used $k = 2/\gamma_{12}$ (Eq (30)). In the limit $x_2 \ll k$ but $x \gtrsim x_2$, the density simplifies to

$$\sigma(x) \approx 2\Gamma x. \tag{80}$$

The linear x-dependence as well as the Γ dependence agrees with numerical results. However, the slope turns out to be too large. This is possibly the consequence of our simplification of the Hamiltonian Eq. (26) to Eq. (27), where all the interaction terms were neglected except for the one between the first and the second levels. As shown in [4], it should be possible to obtain an integral equation for the saddle point density which can then be solved at least approximately.

As we will show, the actual density of the levels play a minor role in the distribution $P(g)$, which is dominated by the first few levels. Therefore our results will be qualitatively correct, although there would be quantitative discrepancies due to the difference in the density.

Note that in the opposite limit $x_2 \gg k$, $x \gg x_2$, the density becomes

$$\sigma(x) \approx 2\Gamma/\gamma_{12}. \tag{81}$$

This corresponds to a uniform average spacing $s = \langle x_{a+1} - x_a \rangle$ of eigenvalues of order unity ($L = L_z$), compared to the uniform spacing $s \approx L_z/\xi$ in Q1D. In contrast, 3D metals are similar to Q1D metals having uniform $\sigma(x)$ extending down to $x = 0$ and $s \sim L_z/L^2$. The opening of a gap in the spectrum of Lyapunov exponents $\nu_n \equiv \langle x_n \rangle / L_z \sim 1/\xi$ may be considered as the signature of the Anderson transition.

VII. RESULTS AND DISCUSSIONS

With the above caveat in mind, the saddle point free energy $F_{sp}(x_1, x_2; g)$ has the form (Eq. (53))

$$F_{sp}(x_1, x_2) = H_1 - \frac{1}{2\gamma_{12}} \int_{x_2}^{b} \frac{dx}{f'(x)} [V'^2(x) - \mu_1^2 h'^2(x)], \tag{82}$$

where primes denote x-derivatives. Eq (55) can then be rewritten as

$$P(\ln g) \propto g \int_{x_{2min}}^{b} dx_2 e^{-F_{sp}(x_1, x_2; g)} e^{-2(x_2 - x_1)}, \tag{83}$$

where the integration over x_1 is eliminated by a constraint arising from the minimization of the free energy:

$$\begin{aligned} x_1 = \;& \cosh^{-1}[1/\sqrt{g - g_0}]; \\ & g_0 = -\tfrac{1}{\gamma_{12}} \textstyle\int_{x_2}^{b} \tfrac{dx}{f'(x)} h'(x)[V'(x) + \mu_1 h'(x)]. \end{aligned} \tag{84}$$

The lower limit x_{2min} is the larger of the additional constraints imposed by the conditions $\sigma(x_2) \geq 0$ and $x_2 > x_1 \geq 0$, x_1 real.

A. Analytical model

It is instructive to consider first a simple approximate solution of Eq. (83), which is dominated by the lower limit of the integral. To a good approximation, g_0 is negligible compared to g in the insulating limit, and $x_1 \approx \frac{1}{2}\ln(4/g)$. The condition $\sigma(x_2) \geq 0$ or equivalently $Y''(x) \geq 0$ gives x_{2min} from the condition $Y''(x_{2min}) = 0$. This gives

$$x_{2min} \approx (1 + \Gamma + \gamma_{12})/2\Gamma \tag{85}$$

and hence $F_{sp} \approx H_1$. This immediately leads to

$$P(\ln g) \propto (4x_{2min}^2 - u^2) e^{-\frac{\Gamma}{4}(\frac{1}{\Gamma} + u)^2}, \quad u \equiv \ln(g/4). \tag{86}$$

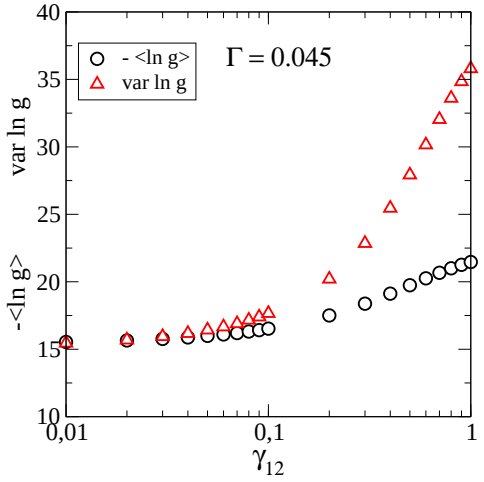

FIG. 22: Mean value $\langle \ln g \rangle$ and variance var $\ln g$ as a function of γ_{12} in the strongly insulating regime, calculated from analytical distribution (83). As expected, var $\ln g \approx -\langle \ln g \rangle$ for $\gamma_{12} \ll 1$ but var $\ln g \approx -2\langle \ln g \rangle$ for $\gamma_{12} = 1$. Note that both mean and variance depends only weakly on γ_{12} when γ_{12} is small (which is always the case when the system size L is large).

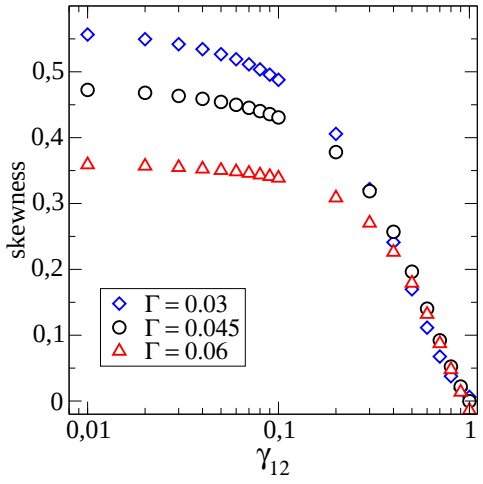

FIG. 23: Skewness as a function of γ_{12} in the strongly insulating regime. As expected, skewness is zero for $\gamma_{12} = 1$ (Q1D limit).

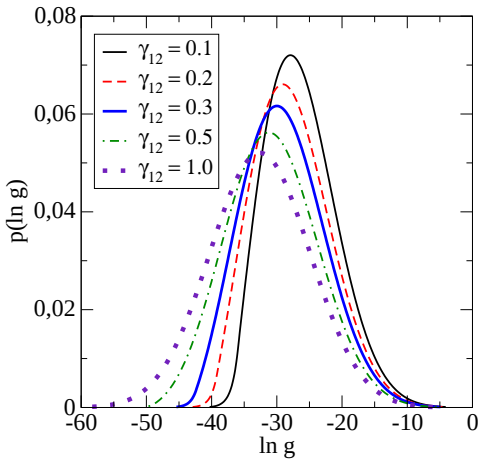

FIG. 24: $P(\ln g)$ obtained from analytical formulas (Eqs. 82, 83 and 84) for $\Gamma = 0.03$ and various values of γ_{12}.

We do a saddle point analysis of Eq. (86) to obtain $\langle \ln g \rangle$ and var$(\ln g)$ as a function of Γ. In order to illustrate the difference between Q1D and 3D insulators, we will keep the general expressions without using the condition $\gamma_{12} \ll 1$. The free energy can be written as

$$F_{approx} = \frac{\Gamma}{4}(x - \frac{1}{\Gamma})^2 - \ln(2x_{2min} - x); \quad x = \ln(1/g). \tag{87}$$

The saddle point solution of the mean $x_m \equiv \langle \ln g \rangle$ is obtained from $F'(x_m) = 0$ where the prime denotes derivative with respect to x. Denoting

$$x_m = 1/\Gamma - y \tag{88}$$

this gives $y(y - \gamma_{12}/\Gamma) = 2/\Gamma$, leading to

$$y = \frac{1}{2}\left[\sqrt{(\frac{\gamma_{12}}{\Gamma})^2 + \frac{8}{\Gamma}} - \frac{\gamma_{12}}{\Gamma}\right]. \tag{89}$$

The variance δx can be estimated from $1/F''(x_m)$, giving

$$\delta x \approx \frac{1}{\frac{\Gamma}{2} + \frac{\Gamma^2 y^2}{4}}. \tag{90}$$

In the limit $\gamma_{12} \to 0$ appropriate for our 3D insulators, $y \to \sqrt{2/\Gamma}$. On the other hand in the Q1D limit $\gamma_{12}^{Q1D} = 1$, $y \to 2$. Thus compared to the Q1D result $\langle \ln g \rangle^{Q1D} \approx 1/\Gamma$, the 3D result is shifted by $\sqrt{2/\Gamma}$. Similarly, compared to the Q1D result var$(\ln g) = 2/\Gamma$, the 3D insulators have a much sharper distribution, with half the variance $1/\Gamma$. Both results agree with numerical data. Although our model is not in general valid for $\gamma_{12} \to 1$ because of our neglect of the interaction terms, in the insulating limit the interaction terms are negligible and it is useful to see how the mean and the variance changes with γ_{12} as it is changed from the 3D limiting value of zero to the Q1D limiting value of unity. Since $\gamma_{12} \sim \xi/2L$, for a given disorder this will correspond to starting from a cubic sample of width $L = L_z \gg \xi$ (where L_z is the length) and decreasing the width to $L < \xi$ to reach the Q1D limit.

Figure 22 shows how the mean and the variance changes with γ_{12} according to Eqs. (88) and (90).

It is not possible to obtain a simple formula for the skewness $\langle (\ln g - \langle \ln g \rangle)^3 \rangle / [\langle (\ln g - \langle \ln g \rangle)^2 \rangle]^{3/2}$ except that in the limit $\Gamma \to 0$ it approaches a number of order unity. Direct evaluation of the quantity as a function of γ_{12} is shown in Fig. 23, which shows that for a given disorder, the skewness starts from zero in the Q1D limit, as is well known, but saturates to a finite value (depending on disorder) in the 3D limit. It shows that the distribution is never log-normal for 3D insulators. It also shows that the

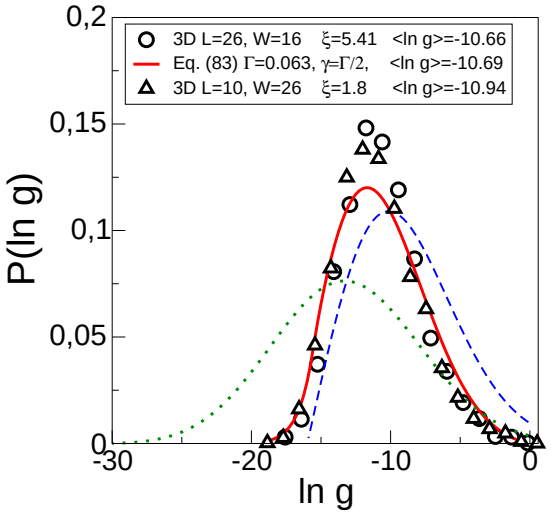

FIG. 25: Conductance distribution for 3D insulators obtained from direct numerical simulation for $W = 16$, $L = 26$ (circles), and from Eq. (83) for $\Gamma = 0.063$ and $\gamma_{12} = \Gamma/2$ (solid line). Both have the same mean value $\langle \ln g \rangle \approx -10.6$. Dashed and dotted lines show Eq. (86) with $x_{2\min} = 1/2\Gamma + 3/4$ and $x_{2\min} = 1/\Gamma$, respectively, with $\Gamma = 0.063$. Shown are also numerical data for $W = 26$ and $L = 10$ (triangles). Similar agreement is obtained for other values of $\langle \ln g \rangle$ if Γ is used as a free parameter; see Ref. [15] for the case $\langle \ln g \rangle \approx -12.6$ fitted with $\Gamma = 0.054$[29].

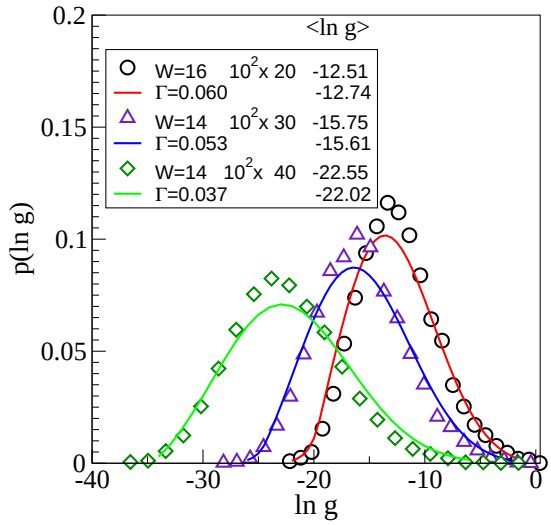

FIG. 26: Conductance distribution for insulating samples of the size $L^2 \times L_z$ ($L = 10$) In contrast to 3D system (fig. 25), parameter $\Gamma/\gamma_{12} < 1$. From numerical data, we have $\Gamma = 0.3$, $\gamma_{12} = 0.22$ for $W = 16$, and $\Gamma = 0.133$ (0.102), $\gamma_{12} = 0.32$ (0.36) for systems with $W = 14$ and $L_z = 30$ (40), respectively. Solid lines show analytical result, Eq. (83) with γ_{12} and $\langle \ln g \rangle$ as given form numerical data.

distribution $P(\ln g)$ is almost independent of γ_{12} provided that both γ_{12} and Γ are small. This explains why the distribution shown in Fig. 25 does not depend on the ratio Γ/γ.

Finally, Fig. 24 shows how the entire distribution $P(\ln g)$ changes as a function of γ_{12}, from a sharp, skewed form for $\gamma_{12} \ll 1$ to a broad Gaussian form for $\gamma_{12} = 1$.

B. Comparison with numerical data

When comparing our theoretical prediction, Eq. (83), with numerical data, we distinguish two cases: (1) for 3D systems, both Γ and γ_{12} decreases $\sim 1/L$, while the ratio Γ/γ_{12} does not depend on L. (2) for systems $L^2 \times L_z$, $\Gamma \sim 1/L_z$ while $\gamma_{12} \sim 1/L$ does not depend on L_z (see fig. 5). Therefore, contrary to 3D geometry, $\Gamma/\gamma_{12} \ll 1$ for $L_z \gg L$. This different behavior of parameters Γ and γ_{12} explains difference between the shape of $p(\ln g)$ in 3D and Q1D strongly disordered systems, shown in figures 25 and 26.

Figure 25 shows Eq. (86) compared with the results from direct integration of Eq. (83), both compared with numerical results based on Eq. (11). For the analytic curves, we chose $\Gamma = 0.063$ and $\gamma_{12} = \Gamma/2$ to have the same $\langle \ln g \rangle$ as in the numerical case[29]. Note that using the Q1D result $\gamma_{12}^{Q1D} = 1$ gives $x_{2min} \approx 1/\Gamma$, leading to a log-normal distribution (see dotted line in Fig. (25)). As shown in [15], variance and skewness calculated from direct integration of Eq. (83) compares well with numerical results, consistent with saddle point results from Eq. (86).

Figure 26 compares theoretical formula, Eq. (83) with numerical data for $p(\ln g)$ for insulating samples $L^2 \times L_z$. While Γ is small, decreasing as $\sim 1/L_z$, γ_{12} does not depend on L_z and is constant for fixed L. Consequently, ratio $\gamma_{12}/\Gamma \sim L_z/L$ increases with increasing L_z.

Both figures 25 and 26 show qualitative agreement with numerical data and theoretical model. Quantitative differences between Eq. (83) and numerical results have origin in our simplified model Eq. (19), which still overestimates the strength of the interaction for higher channels.

It is important to note that in both figures 25 and 26 we compared numerical data with theoretical model with the same mean $\langle \ln g \rangle$. This is consistent with scaling theory of localization since there is only one parameter - for instance $\langle \ln g \rangle$ - which determines $p(\ln g)$ completely. In order to make sure that the analytical model has the same $\langle \ln g \rangle$ as the numerical data for a given disorder, we used Γ as a free fitting parameter. Of course we could use Eq. (20) to obtain Γ independently for a given disorder. However, in order to do that we will need a good estimate of the mean free path ℓ. This is difficult in the strongly disordered regime because the mean free path defined as the decay length of the single particle Green's function is actually smaller than the lattice spacing in the strongly disordered regime[31], and our numerical model does not allow us to obtain such small lengths with good accuracy. While independent calculations of the mean free path are available for cubic systems below critical disorder[31] (e.g.

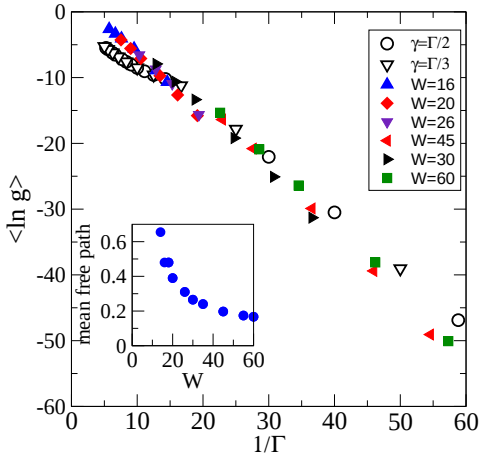

FIG. 27: Mean value $\langle \ln g \rangle$ as a function of $1/\Gamma$. Open symbols: analytical result, Eq. (83). Data confirm linear dependence $\langle \ln g \rangle \propto 1/\Gamma$ for small Γ (strong disorder). For smaller disorder (larger Γ) analytical model is less accurate. Data confirm that $\langle \ln g \rangle$ does not depend on γ_{12} provided that both Γ and γ_{12} are small. Full symbols: numerical data with $\Gamma^{-1} = LK_{11}/\ell$. We estimate Γ for a given disorder using the mean free path ℓ obtained from data in fig. 19a ($\ell(W)$ is shown in inset) and the relation $K_{11}L = x_1\ell$. Numerical $\langle \ln g \rangle$ is an unambiguous function of Γ, as required in the analytical model. Small deviations are due to finite size effects which affect actual values of parameters x_1 and K_{11}.

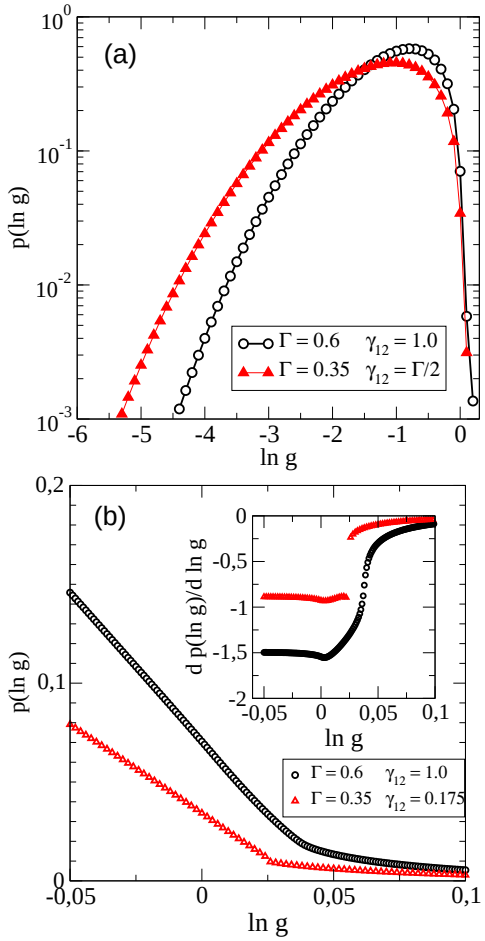

FIG. 28: (a) Probability distribution $P(\ln g)$ for $\Gamma \sim 1$ where critical regime is expected. The distribution agrees qualitatively with numerical data for the critical regime. Figure (b) shows detail of the distribution shown for $\Gamma = 0.35$, $\gamma_{12} = \Gamma/2$ and for $\Gamma = 0.6$, $\gamma_{12} = 1$. It shows that there is indeed a non-analyticity in the distribution close to $\ln g = 0$ with position of the non-analyticity at $\ln g > 0$, in agreement with analytical results[6].

$\ell = 0.234$ for $W = 15$ in the isotropic case), there is no data available in the insulating regime. We therefor use Γ as a free parameter. Nevertheless, as a consistency check, we estimate ℓ from a plot of $K_{11}L$ vs x_1 (fig. 19a), where the slope should give the mean free path (equivalently, we could identify Γ^{-1} with numerical value of x_1). The results are plotted as the inset in fig. 27 to show the mean free path as a function of disorder. Using this result, we can estimate the value of Γ corresponding to the disorder $W = 16$ used in fig. 25. We find that $\ell(W = 16) \approx 0.48$ and $\Gamma = 0.070$, which is close to the fitting value 0.063. This shows that while we can not obtain Γ accurately enough in our present numerical scheme, the fitted values are consistent with our crude estimates. As a further consistency check, we use the above estimate of the mean free path to plot in fig. 27 the Γ dependence of $\langle \ln g \rangle$. It shows that $\langle \ln g \rangle$ is indeed an unambiguous function of Γ, as required by the theory.

Finally, we have checked the effects of fluctuations of k_{11} on $P(\ln g)$ by integrating the conductance distribution in fig. 25 over the distribution $P(k_{11})$ (fig. 4). We find that the effects are negligible.

VIII. BEYOND THE INSULATING LIMIT

From numerical simulations[7,8] we know that the critical regime in 3D is also dominated by only a few eigenvalues $x_i \gg 1$. However, since γ_{12} is neither 0 nor 2, it seems that we may not be able to use the free fermion ($\eta = 0$) solution of Eq. (24) to obtain the distribution of the transmission levels. However, as shown in [32], the solution is independent of the strength of the interaction η in the strong disorder regime characterized by $x_i \gg 1$. This means that our solutions might be used, albeit only qualitatively, even near the critical regime. We show in Fig. (28) the distribution $P(\ln g)$ for $\Gamma \sim 1$ which is expected to be near the critical regime. It agrees qualitatively well with numerical results at the critical point, including a discontinuity in the slope near $g = 1$. It is known from analysis of the Q1D systems[6] that separating out an additional level helps to study the non-analyticity near $g = 1$. We therefore expect to obtain better results near the critical regime by separating out an additional level.

Finally, we show in Fig. 29 the distribution $P(g)$ for

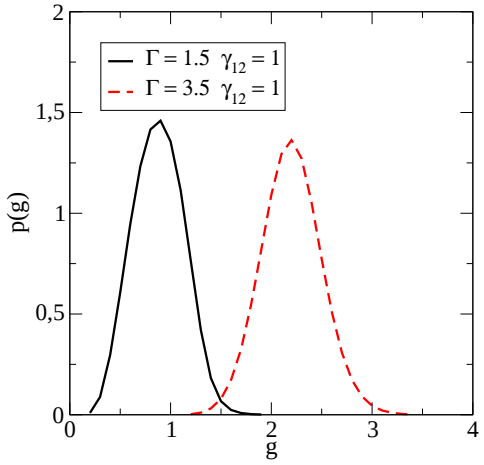

FIG. 29: Analytic result for the metallic regime ($\Gamma > 1$ and $\gamma_{12} = 1$). Data confirm that the distribution $P(g)$ is Gaussian with variance var $g = 0.064$ for $\Gamma = 1.5$ and var $g = 0.09$ for $\Gamma = 3.5$ which is comparable to the UCF value.

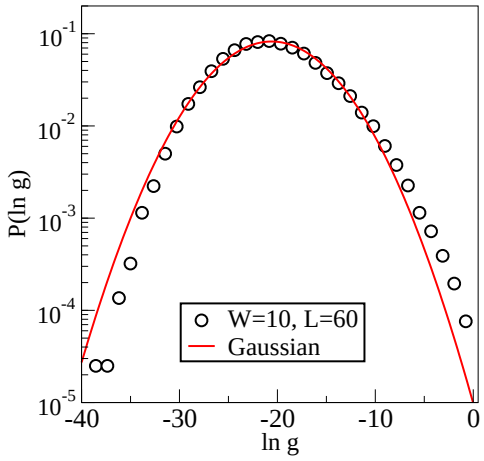

FIG. 30: Typical form of the distribution $p(\ln g)$ in 2D disordered systems compared with Gaussian distribution with the same mean value and variance. $\langle \ln g \rangle = -20.6$, var $\ln g = 23.5$ and skewness is 0.251. Figure indicates that the deviation from the Gaussian distribution exists in 2D as well.

$\Gamma > 1$ and for $\gamma_{12} = 1$ which corresponds to the metallic regime. Although we do not expect that our approximate formula works quantitatively for the metallic regime, Eq. (83) gives, for this choice of the parameters, a Gaussian distribution of the conductance. Also the width of the distribution qualitatively agrees with the universal conductance fluctuations[33] in this regime. This shows that our simple model already captures the essential qualitative features at all strengths of disorder.

IX. SUMMARY AND CONCLUSION

We systematically analyzed the length and disorder dependence of the matrix K to check if the generalized DMPK equation proposed in [14] is valid in three dimensional systems at all strengths of disorder.

We studied the matrix K in detail. The goal was to test the assumptions on which the generalized DMPK equation was derived and to construct a simple analytically tractable model for K which captures all the important qualitative features. In particular, since Q1D systems have been studied in great detail, we looked for any major qualitative differences in the structure of K between Q1D and 3D systems.

We find that to a good approximation, the generalized DMPK equation remains *qualitatively* valid for any disorder. We also conclude that to a good approximation, we can use only two parameters, $K_{aa} \approx K_{11}$ and $\gamma_{ab} \approx \gamma_{12}$, to characterize the qualitative changes in transport at different strengths of disorder in different dimensions. We find that although fluctuations in k_{11} at strong disorder are large (non self-averaging), the effect of these fluctuations on $P(\ln g)$ is negligible. More importantly, we do not have an independent way to estimate the mean free path to obtain $\Gamma = \ell/(L_z K_{11})$, but all qualitative features of the entire distribution $P(\ln g)$ is obtained correctly once an effective Γ is used as a free parameter. We also find how these parameters depend on disorder and show their unambiguous dependence on the localization length. This is important since it indicates that the introduction of new parameters does not necessarily invalidate the single parameter scaling theory of localization.

We have also shown that the matrix K contains information about the Anderson transition. The scaling of the parameters LK_{11} or γ_{12} clearly identifies the critical point which agrees with numerical results.

We then concentrate on the strong disorder limit where our numerical results allowed us to construct a simple *one-parameter model* of the matrix K, containing $\Gamma = \ell/K_{11}L_z$ and $\gamma_{12} = 2K_{12}/K_{11}$, with $\Gamma/\gamma_{12} = 2$. By varying γ_{12}, we show how one can go from a Q1D ($\xi \gg L$) to a truly 3D ($\xi \ll L$) system in the insulating regime, which clearly shows the difference between a Q1D and a 3D insulator. We then use the model to obtain the full distribution $P(g)$ which agrees qualitatively with numerical results.

It is indeed remarkable that even though the generalized DMPK equation (22) neglects fluctuations in k_{ab} and the model Eq. (19) neglects the index dependence of K_{ab}, the theory still captures all the essential features of length, disorder as well as dimensionality dependence of the entire conductance distribution and provides in particular a simple understanding of the 3D distribution at strong disorder, which is qualitatively different from a log-normal distribution in Q1D. At the same time, our numerical studies suggest that having an independent estimate of the mean free path could provide a more quantitative description of the conductance distribution in 3D at all disorder.

We emphasize that there are large differences between Q1D and higher dimensions. In Q1D defined in [4,5,6,18],

disorder is always *weak* enough to assure that the localization length $\xi \gg L$ where L is the transverse dimension. The Q1D insulator corresponds to the *weakly disordered* systems of length $L_z \gg \xi$. It is this length-induced insulating behavior that is described by the DMPK equation. This is different from localization in 3D which occurs at *strong* disorder, where ξ is much less than both L_z and L. This difference is clearly reflected in the matrix K, where Table I summarizes how the scale dependence of K_{11} and γ_{12} depend on disorder in 3D. In contrast, K in Q1D is independent of disorder. Our model recovers all the peculiarities of the 3D localized regime: we found that the distribution $P(\ln g)$ is narrower than in Q1D and possesses non-zero skewness.

Although we concentrated on 3D systems, general considerations about the properties of the matrix K in the insulating regime should be valid in any dimension $d > 2$. In particular, the assumption that K_{11} is a nonzero L-independent constant in the localized regime is correct independent of dimensionality. Therefore, we expect that our theory of the insulating regime is valid for any $d > 2$. Consequently, the distribution $P(\ln g)$ is not Gaussian in the localized regime in any $d > 2$, although the nature of the deviation from the Gaussian form might be dimensionality dependent. In fact we expect $P(\ln g)$ to be different from Gaussian distribution even in 2D[11]. This expectation is supported by Fig. 30 which shows $P(\ln g)$ for a 2D square system obtained numerically using Eq. 11. As discussed in the paper, deviations from the Gaussian form are due to the changes of the spectrum of parameters x. Although the contribution of the first channel to the conductance is dominant, higher channels do influence the statistical properties of the smallest parameter, x_1. This effect was probably not considered in previous analytical works which predict Gaussian distributions of $\ln g$ in the insulating regimes in dimensions $d = 2 + \epsilon$[12].

When applied to the critical regime, our theory recovers typical properties of the conductance distribution, including the non-analyticity of the distribution in the vicinity of $g = 1$. Although our present results are only qualitatively correct in the critical regime, we believe that the method developed in the paper represents a good starting point for further development of the theory of Anderson transition.

KAM thanks U. Karlsruhe for support and hospitality during his visit. PM thanks APVT, grant n. 51-021602 for financial support. PW gratefully acknowledges support of a visit and hospitality at the U. Florida as well as partial support by a Max-Planck Research Award.

[1] K. A. Muttalib, P. Wölfle and V. A. Gopar, Ann. Phys. **308**, 156 (2003).

[2] J.-L. Pichard, in B. Kramer (ed.) *Quantum Coherence in Mesoscopic Systems* NATO ASI **254**, Plenum Press NY and London (1991).

[3] A. García-Martin and J. J. Sáenz, Phys. Rev. Lett. **87**, 116603 (2001); A. García-Martin, M. Governale and P. Wölfle, Phys. Rev. B **66**, 233307 (2002);

[4] K. A. Muttalib and P. Wölfle, Phys. Rev. Lett. **83**,3013 (1999); P. Wölfle and K.A. Muttalib, Ann. Phys. (Leipzig) **8**, 753 (1999).

[5] V. A. Gopar, K. A. Muttalib and P. Wölfle, Phys. Rev B **66**, 174204 (2002); L. S. Froufe-Perez, P. García-Mochales, P. A. Serena, P. A.Mello and J. J. Sáenz, Phys. Rev. Lett. **89**, 246403 (2002) .

[6] K. A. Muttalib, P. Wölfle, A. Garcia-Martin and V. A. Gopar, Europhys. Lett. **61**, 95 (2003); A. García-Martin and J. J. Sáenz, Phys. Rev. Lett. **87**, 116603 (2001).

[7] P. Markoš and B. Kramer, Philos. Mag. B **68**, 357 (1993);

[8] P. Markoš, Phys. Rev. Lett. **83**, 588 (1999); M. Rühländer, P. Markoš and C.M. Soukoulis, Phys. Rev. B **64**, 212202 (2001).

[9] B. K. Nikolic, P. B. Allen, Phys. Rev. B **63**, 020201 (2001); M. Rühländer, P. Markoš and C.M. Soukoulis, Phys. Rev. B **64**, 172202 (2001);

[10] K. Slevin, P. Markoš and T. Ohtsuki, Phys. Rev. Lett. **86**, 3594, (2001)

[11] P. Markoš, Phys. Rev. B **65**, 104207 (2002); P. Markoš in *Anderson Transition and its Ramifications*, eds. T. Brandes and S. Ketteman, Lecture Notes in Physics vol. 630, Springer 2003.

[12] B.L. Altshuler, V.E. Kravtsov and I. Lerner, Sov. Phys. JETP **64**, 1352 (1986), and Phys. Lett. A **134**, 488 (1989).

[13] B. Shapiro, Phys. Rev. Lett. **65**, 1510 (1990); A. Cohen and B. Shapiro, Int. J. Mod. Phys. B **6**, 1243 (1991).

[14] K. A. Muttalib and V. A. Gopar, Phys. Rev B **66**, 115318 (2002); K. A. Muttalib and J. R. Klauder, Phys. Rev. Lett. **82**, 4272 (1999).

[15] P. Markoš, K. A. Muttalib, P. Wölfle and J. R. Klauder, Europhys. Lett. **68**, 867 (2004)

[16] E. Abrahams, P. W. Anderson, D. C. Licciardello, T. V. Ramakrishnan, Phys. Rev. Lett. **42**, 673 (1979); A. MacKinnon, B. Kramer, Phys. Rev. Lett. **47**, 1546 (1981).

[17] See e.g. A. D. Stone, P. Mello, K. A. Muttalib and J-L. Pichard in *Mesoscopic phenomena in solids*, eds. B. L. Altshuler, P. A. Lee and R. A. Webb, North-Holland, 369 (1991).

[18] O. N. Dorokhov, JETP Lett. **36**, 318 (1982); P. A. Mello, P. Pereyra and N. Kumar, Ann. Phys. (N.Y.) **181**, 290 (1988).

[19] R. Landauer, IBM J. Res. Dev. **1**, 223 (1957).

[20] For a recent review, see Ya.M. Blanter and M. Büttiker, Phys. Rep. 336, 1 (2000).

[21] C.W.J. Beenakker, Phys. Rev. B 46, R12841 (1992).

[22] $T^\dagger T = \frac{1}{4}[M^\dagger M + (M^\dagger M)^{-1} - 2]$, see J.-L. Pichard in [2].

[23] I. Zambetaki, Q. Li, E. N. Economou and C. M. Soukoulis, Phys. Rev. Lett. **76**, 3614 (1996).

[24] J. B. Pendry, A. MacKinnon, and P. J. Roberts, Proc. R. Soc. London A **437**, 67 (1992). T. Ando, Phys. Rev. B **44**, 8017 (1989)

[25] J.-L. Pichard, N. Zannon, Y. Imry, J. Phys. France **51**, 587

(1990).
[26] J.T. Chalker and M. Bernhardt, Phys. Rev. Lett. **70**, 982 (1993).
[27] Note that for $|a-b| \gg L$, γ_{ab} must decrease as L^{-2}. Indeed, from (8) we have $\sum_b K_{ab} = 1$ so that the sum of L^2 *positive* parameters $\sum_b \gamma_{ab}$ is $\propto L^0$ in the insulating regime. We ignore this detail in our model.
[28] P. Markoš J. Phys.: Condens. Matt. **7**, 8361 (1995).
[29] In Ref. [15] we used $\Gamma/\gamma_{12} = 4$. This difference is not important, since, as we show in Fig. 23, the actual value of Γ/γ_{12} does not influence the value of the skewness when both Γ and γ_{12} are small.
[30] C. W. J. Beenakker and B. Rejaei, Phys. Rev. Lett. **71**, 3689 (1993); Phys. Rev. B **49**, 7499 (1994).
[31] E. N. Economou, C. M. Soukoulis and A. D. Zdetsis, Phys. Rev. B 31, 6483 (1985).
[32] M. Caselle, Phys. Rev. Lett. 74, 2776 (1995).
[33] B.L. Altshuler, JETP Lett. 41, 648 (1985); P.A. Lee and A.D. Stone, Phys. Rev. Lett. 55, 1622 (1985).